INTERNATIONAL JOURNAL of RENEWABLE ENERGY RESEARCH
S. Mamidala and Y. V. P. Kumar, Vol.16, No.1, March, 2026

Critical Review of Key DC-DC Converters for Maximum Power Extraction in Solar-Powered Electric Vehicle Charging Stations

Sugunakar Mamidala, Y. V. Pavan Kumar‡

School of Electronics Engineering, VIT-AP University, Amaravati 522241, Andhra Pradesh, INDIA

(sugunakarmamidala.20phd7113@vitap.ac.in, pavankumar.yv@vitap.ac.in)

‡Corresponding Author; Y. V. Pavan Kumar, VIT-AP University, Amaravati 522241, Andhra Pradesh, INDIA, Tel: +91 863-2370155, pavankumar.yv@vitap.ac.in

Received: 09.02.2024 Accepted: 10.03.2024

Abstract - Integrating solar photovoltaic (PV) systems into charging stations of electric vehicles (EVs) presents a viable option for improving energy efficiency and decreasing dependence on traditional grid sources. However, the effectiveness of the PV system relies on the selection of a suitable DC-DC converter along with the maximum power point tracking (MPPT) methodology. Generally, there are five key DC-DC converters (namely buck-boost, Cuk, SEPIC, zeta, and flyback converters) and two MPPT methods (namely perturb and observe (P&O) and incremental conductance (INC) methods) have been developed in the literature for different renewable energy applications in different scenarios. However, an effective combination of the converter and MPPT method for PV-based EV charging station application was not identified in the literature. Thus, this paper performs a critical review of all the key DC-DC converters and MPPT methods that are given above and identifies the best combination that optimally extracts maximum power from solar PV panels. For the performance comparison, various parameters, namely solar power extraction, converter output voltage, and converter efficiency, are computed under diverse test conditions, including irradiance, temperature, and the electric vehicle's battery state of charge (SOC). The system design has been carried out in MATLAB/Simulink software. The outcomes of this research work explore the flyback converter as superior to other converters when it is combined with P&O-based MPPT. Thus, this work provides valuable insights into the investigation of an efficient DC-DC for solar-powered electric vehicles, fostering advancements in renewable energy utilization for automotive applications.

Keywords: Charging station, DC-DC converter, electric vehicles, EV battery, MPPT algorithm, PV system.

1. Introduction

Energy independence is promoted through the advancement of battery technology and charging infrastructure, which allows for charging from different sources, such as renewable sources [1, 2]. The popularity of electric vehicles (EVs) is increasing due to their sustainability, cost savings, and innovation. The advantages of each EV type, including battery-based electric vehicles, plug-in-based electric vehicles, and hybrid electric vehicles, include quiet operation, zero emissions, and eco-friendly trends [3-7]. The attractiveness of electric vehicles lies in their ability to withstand fuel price fluctuations and their dependence on stable electricity costs. The charging infrastructure plays a vital role in addressing range anxiety. The benefits of EV adoption extend to environmental sustainability, economic appeal, technological innovation, and societal trends, painting a compelling picture of the future of cleaner, more efficient, and environmentally conscious mobility [8, 9].

The growing demand for clean transportation is met by the global expansion of EV charging stations. This infrastructure requires the DC-DC converter, which acts as a vital link between the electric grid and EV batteries [10, 11]. To ensure optimal charging conditions, it is crucial to efficiently convert and match voltage levels. The converter can ensure seamless connections with varying grid voltages by tailoring the grid voltage to meet specific EV battery

requirements, which is crucial for grid compatibility [12, 13]. The DC-DC converter in fast-charging stations is capable of handling higher power levels, which leads to efficient rapid charging [14]. The charging process is aligned with battery specifications by integrating with the EV's battery management system. In addition to charging, it permits bidirectional energy flow for vehicle-to-grid applications, permitting electric vehicles to release their stored energy during peak demand [15, 16]. The DC-DC converter is an essential piece of the infrastructure that supports widespread EV adoption through efficiency, adaptability, and future-ready technology.

The use of the electrical grid can be significantly decreased by combining solar systems with electric vehicles, which provides a sustainable and distributed energy source [17]. Solar systems generate clean, independent electricity for EV charging and reduce reliance on the grid, especially during peak demand [18, 19]. Energy independence is achieved for homeowners who install solar panels, which means they rely less on the central grid for their daily needs, including EV charging. Solar systems help reduce peak demand by producing the most energy during daylight hours, which aligns with peak demand periods [20]. A more distributed and resilient energy network can be achieved by using solar installations collectively in multiple homes and businesses to reduce the load on the centralized grid [21]. The use of excess solar energy for EV charging during non-sunlight hours is made possible by combining solar systems with battery storage, which reduces the need for grid-based electricity. The integration of smart inverters and grid management systems allows solar systems to provide load balancing and grid support services [22, 23], which stabilize the grid by adjusting electricity flow depending on demand.

The addition of a DC-DC converter with a solar system is essential for optimizing energy conversion. This converter dynamically adjusts voltage to align with battery or DC load requirements, maximizing energy transfer efficiency, especially in varying sunlight conditions. It plays a pivotal role in minimizing energy losses and enhancing overall system performance, which is a key aspect when solar panels operate below their maximum power point [24]. The converter in solar systems with energy storage ensures that the system is flexible for diverse applications by preventing overcharging or undercharging. Grid-tied systems ensure seamless compatibility, facilitating the smooth exchange of energy without any interruptions. The DC-DC converter plays a vital role in solar energy systems by incorporating remote monitoring and control features, enhancing overall operational efficiency [25]. A significant challenge in this context is the optimization of maximum power extraction from the solar photovoltaic (PV) system discussed in [26]. To address this challenge, perturb and observe (P&O) and incremental conductance (INC) based maximum power point tracking algorithms have been employed [27-30].

Considering all the above-mentioned advancements and limitations of the literature, this paper performs a critical review of all the key DC-DC converters (namely Buck-Boost, Cuk, SEPIC, Zeta, and Flyback converters) and two MPPT methods (namely INC and P&O) that are available in the literature. Further, this paper identifies the best combination that optimally extracts maximum power from solar PV panels that are integrated into electric vehicle charging stations. It is to be noted that this paper is neither a review of the existing literature nor a bibliographic review. It is an experimental verification of the abovementioned DC-DC converters and MPPT methods to find their applicability to electric vehicle charging stations.

System simulations and comparative analysis are performed using MATLAB/Simulink software. Various real-time test cases with varying environmental conditions (namely irradiance and temperature) and EV load conditions (namely battery state of charge (SOC)) are implemented for validating the converters and MPPT methods. The comparison is done by calculating various performance parameters, namely solar power, converter output voltage, and converter efficiency. These contributions collectively enhance the understanding and practical application of solar energy in the context of developing EV charging stations. The rest of the paper is organized as follows.

Section 2 describes the operation of solar-powered EV charging stations. Section 3 explains the modelling of the considered DC-DC converters to be used for the development of charging stations. Section 4 discusses the MPPT techniques and their implementation procedures, Section 5 presents the findings and comparative analysis, and Section 6 provides the conclusion of this article.

2. Operation of Solar-Powered EV Charging Station

The architecture of the solar-powered EV charging station embodies a forward-looking vision for the future of eco-friendly and efficient transportation. Through the careful integration of a solar PV system, sophisticated MPPT techniques, DC-DC converters, and electric vehicles depicted in Fig. 1, this charging station signifies a significant advancement in reshaping the landscape of sustainable electric mobility. This comprehensive approach represents a pivotal shift in the way we perceive and harness clean energy for electric vehicles, marking a noteworthy stride in the paradigm of sustainable transportation.

Solar power generation is influenced by environmental factors, including daily irradiation and temperature variations. This intermittency results in energy output fluctuations, posing challenges for a reliable charging service. To overcome this, integrating diverse technologies like MPPT methods, DC-DC converters, and smart grid systems is essential, but presents some technical challenges. Achieving seamless compatibility/effective communication among these systems demands meticulous planning, solving complexities in their integration. In the system architecture, the MPPT controllers sense the voltage and currents from the solar panels and generate switching pulses directed to DC-DC converters, ensuring a steady voltage for recharging EVs. The modelling of PV cells is given as follows.

The solar PV module is the primary power generation source for solar-powered EV charging stations. Modelling of PV cells plays a key role in sizing the solar power system to meet the specific needs of the EV charging station [31].

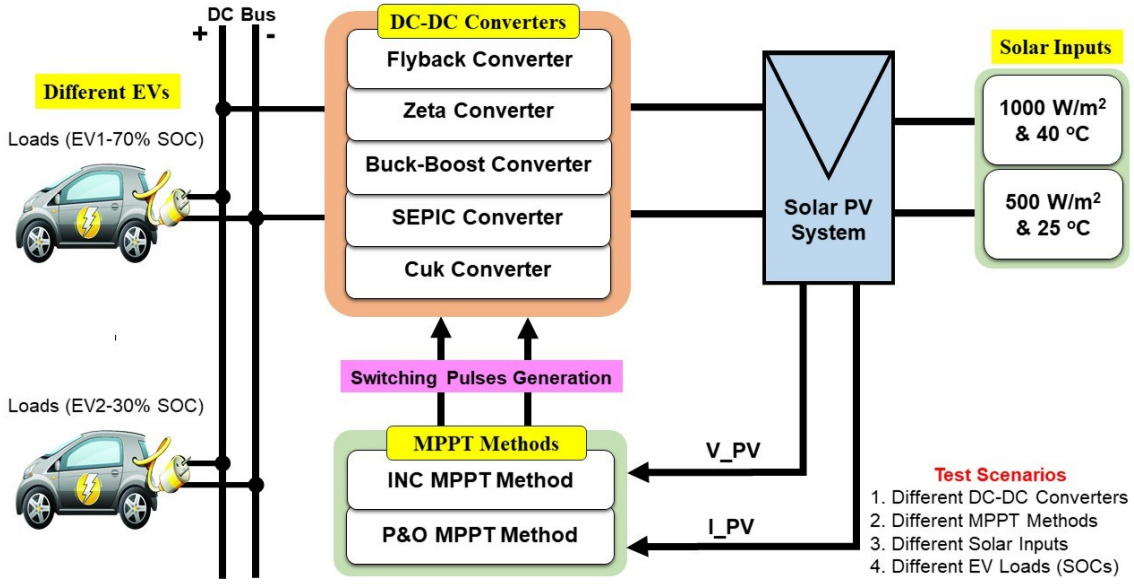

Fig. 1. The architecture of the solar charging station with an indication of various test scenarios.

The widely adopted single-diode model incorporates fundamental electrical components, including a diode, light-generated current, series resistance, and shunt resistance, as illustrated in Fig. 2(a). The voltage and current relationships within the PV cell model are expressed as given in Eq. (1). To maximize the power output, a solar cell needs to be operated at its optimal voltage (V_{opt}) and current (I_{opt}), combinedly known as the maximum power point (MPP). As shown in Fig. 2(b), the I-V and P-V characteristics of the solar cell are obtained by employing Eq. (1). From this, the maximum power (P_{mp}) is computed as given in Eq. (2) at the optimal value of both voltage/current.

$$\left.\begin{aligned} I_{pv} &= I_{ph} - I_{sh} - I_d \\ &\text{where} \\ I_{sh} &= \frac{V_{pv} + I_{pv}R_{se}}{R_{sh}} \\ I_d &= I_o\left(e^{q\left(V_{pv}+I_{pv}R_{sh}\right)/nkT} - 1\right) \\ V_{pv} &= \frac{nkT}{q}\ln\left(\frac{I_{ph}-I_{pv}}{I_o}\right) \end{aligned}\right\} \quad (1)$$

$$\text{Maximum Power Extraction } \left(P_{mp}\right) = I_{opt} \times V_{opt} \quad (2)$$

Where the output current is denoted as I_{pv}, representing the overall current output. I_d signifies the diode current, while I_{sh} stands for the shunt resistance current. I_{ph} is used to represent the light-generated current, and I_o is associated with the reverse saturation current. The elementary charge is represented by q, and V_{pv} indicates the voltage across the terminals. The ideality factor is denoted as n, and Boltzmann's constant is represented by k. T stands for the absolute temperature, and R_{se} represents the series resistance, whereas R_{sh} signifies the shunt resistance.

3. Modelling of DC-DC Converters for Charging Station

The DC-DC converter is a pivotal component in EV charging stations, bridging the balance between the power supply system and the battery [32].

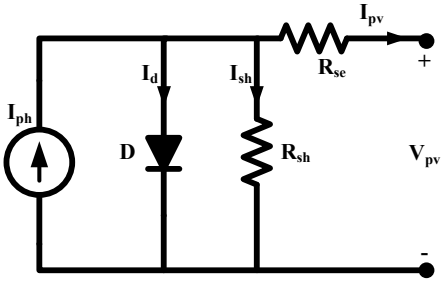

(a) Equivalent circuit

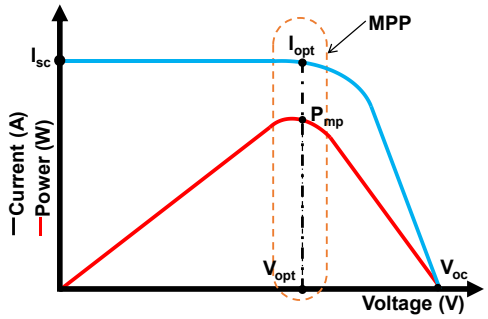

(b) P-V and I-V characteristics

Fig. 2. PV cell equivalent circuit and characteristics.

Its primary role is to efficiently convert and align voltage levels, ensuring optimal charging conditions. Moreover, it adapts the incoming supply voltage to match the charging specifications of various EV models. This research delved into the integration of Cuk, SEPIC, Buck-boost, Zeta, and Flyback converters with a solar system to maximize power extraction. The high-level block diagram of solar-powered EVs with various DC-DC converters that are operated with both INC and P&O MPPT controllers is depicted in Fig. 3(a) to Fig.3(e).

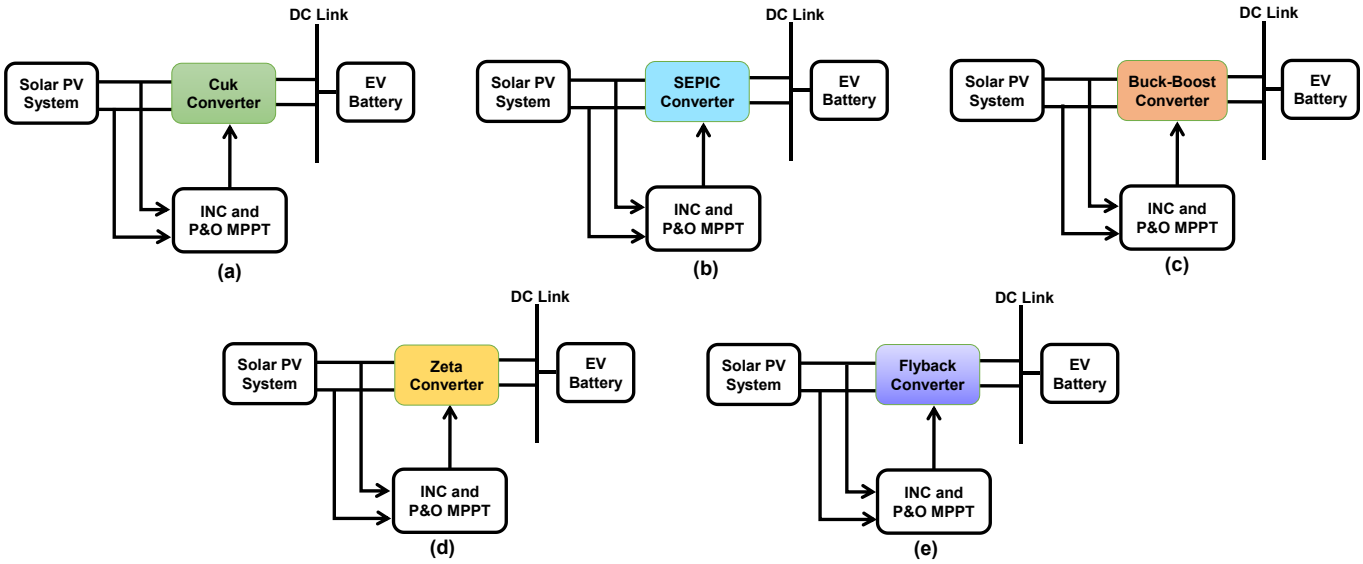

Fig. 3. Block diagrams of the EV charging system with different DC-DC converters.

3.1. Solar Powered Cuk Converter

The Cuk converter is a specialized DC-DC converter designed for efficient EV charging by maintaining a desired output voltage (V_{out}) for battery charging. The duty cycle (D) is regulated by INC and P&O MPPT controllers to ensure a consistent output voltage. Its intricate design addresses the unique requirements of EV charging, making it a key component in advancing EV charging technology for optimal power delivery. The Cuk converter operates in four modes of operation to analyze the performance [33].

- **Mode-1 (Switch Q is ON, 0 < t < DT)**: At the beginning, there is no stored charge in the capacitors and inductors of the Cuk converter. In this mode, the inductor current (I_{L1}) begins to rise and accumulate energy with a positive-to-negative polarity in alignment with the input current (I_{in}). The direction of the current flows toward the switch Q, and then returns to the source as shown in Fig. 4(a). The inductor L_1 current is calculated from Eq. (3).
- **Mode-2 (Switch Q is OFF, DT < t < T)**: Once the switch Q is turned OFF after half cycle, the previously charged inductor current is discharged in the reverse direction and hence the input voltage is added to the inductor voltage (V_{L1}), and the current starts flowing through the capacitor C_1 and makes the diode D is in forward biased. The direction of the current is given in Fig. 4(b). Using this, the inductor current is computed as given in Eq. (4).
- **Mode-3 (Switch Q is ON)**: The inductor (L_1) is charging, and the previously charged capacitor (C_1) is discharging through EV loads when the switch (Q) is turned ON again in Mode-3. The reverse direction of the capacitor current makes the diode (D) reverse-biased, and the direction of the current is from Q, C_2, EV loads, and L_2 as shown in Fig. 4(c). The inductor L_2 voltage and capacitor C_1 and C_2 currents are calculated from Eq. (5) - Eq. (7).
- **Mode-4 (Switch Q is OFF):** The switch Q is turned OFF and repeats the Mode-2 operation. The previously charged inductor L_2 is discharging through the diode D and transfers the energy to EV loads as shown in Fig. 4(d), and the output voltage is calculated from Eq. (8). The average value of L_1 and L_2 inductors' voltage in ON and OFF modes of operation are given by Eq. (9) and Eq. (10) respectively. Finally, the voltage output of the converter is given as Eq. (11).

$$V_{L1} = L_1\left(\frac{dI_{L1}}{dt}\right) = V_{in} \Rightarrow \frac{dI_{L1}}{dt} = \frac{V_{in}}{L_1} \tag{3}$$

$$\frac{dI_{L1}}{dt} = \frac{V_{L1}}{L_1} = \frac{V_{in} - V_{C1}}{L_1} \tag{4}$$

$$\frac{dI_{L2}}{dt} = \frac{V_{L2}}{L_2} = \frac{-(V_{C1} + V_{out})}{L_2} \tag{5}$$

$$\frac{dV_{C1}}{dt} = \frac{I_{C1}}{C_1} = \frac{I_{L2}}{C_1} \tag{6}$$

$$\left.\begin{aligned} &I_{C2} = I_{L2} - I_{out} \quad \text{and} \quad C_2\frac{dV_{C2}}{dt} = I_{L2} - \frac{V_{out}}{R_{load}} \\ &\Rightarrow \frac{dV_{C2}}{dt} = \frac{I_{L2}}{C_2} - \frac{V_{out}}{C_2 \times R_{load}} \end{aligned}\right\} \tag{7}$$

$$V_{L2} = -V_{out} \Rightarrow \frac{dI_{L2}}{dt} = \frac{-V_{out}}{L_2} \tag{8}$$

$$\left.\begin{aligned} &V_{L1} = 0 = DV_{in} + (1-D)(V_{in} - V_{C1}) \\ &\Rightarrow V_{C1} = \frac{V_{in}}{1-D} \end{aligned}\right\} \tag{9}$$

$$\left.\begin{aligned} &V_{L2} = 0 = -D(V_{C1} + V_{C2}) - (1-D)(V_{C2}) \\ &\Rightarrow V_{C2} = -V_{C1}(D) \end{aligned}\right\} \tag{10}$$

$$V_{C2}(=V_{out}) = \left(-\frac{D}{1-D}\right)V_{in} \tag{11}$$

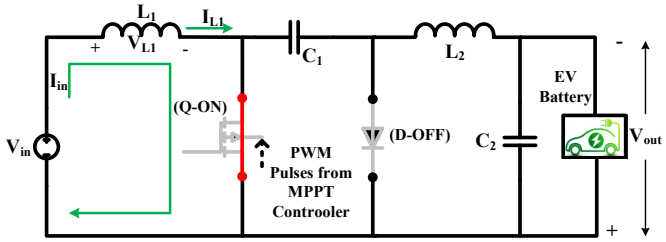

(a) Mode-1

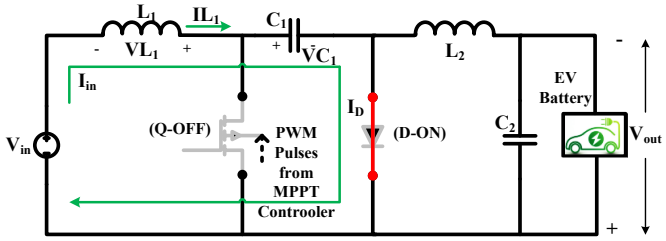

(b) Mode-2

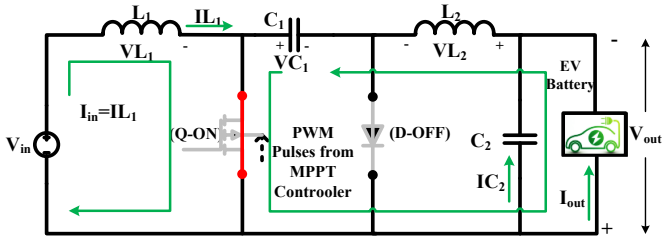

(c) Mode-3

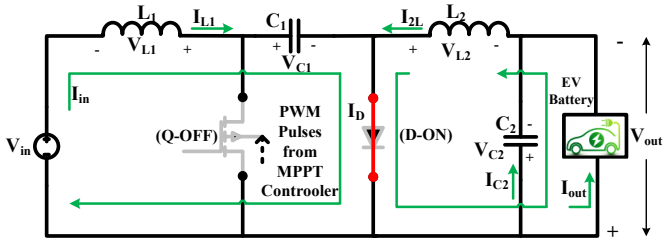

(d) Mode-4

Fig. 4. Current flow in the Cuk converter during the switch ON and OFF states in various modes.

3.2. Solar Powered SEPIC Converter

The SEPIC converter is a versatile DC-DC converter with the capability for both step-up and down the input voltage. The converter provides a non-inverted output and ensures electrical isolation between the input and output. The primary purpose is to stabilize and regulate the output voltage despite fluctuations in the input voltage [34]. The converter's switch is governed by the duty cycle (D), generated by the INC and P&O MPPT controllers to maintain the constant output voltage at the DC link.

- **Mode-1 (Switch Q is ON, 0 < t < DT):** The switch Q is turned ON by applying gate pulses from the MPPT controller, and the inductor L_1 starts charging from the input current (I_{in}). At this instant, the inductor voltage (V_{L1}) is nearly equal to the source voltage (V_{in}). The direction of the input current flows through inductor L_1, switch Q, and returns to the source. Thus, the inductor L_2 is also charged by the capacitor C_1 as shown in Fig. 5(a). The inductor voltages and capacitor current are computed by Eq. (12) and Eq. (13).

$$V_{L1} = V_{in} \text{ and } V_{L2} = V_{C1} \tag{12}$$

$$I_{C2} + I_{out} = 0 \Rightarrow I_{C2} = -I_{out} = -\frac{V_{out}}{R_{load}} \tag{13}$$

- **Mode-2 (Switch Q is OFF, DT < t < T)**: In this mode, the inductor L_1 doesn't allow a sudden change in current. Thus, the inductor starts discharging in the reverse direction and supplies energy to the capacitor C_1 as shown in Fig. 5(b). The inductor voltages and capacitor currents are calculated from Eq. (14) to Eq. (17).

$$\left.\begin{aligned} -V_{in} + V_{L1} + V_{C1} + V_{out} = 0 \Rightarrow V_{L1} = V_{in} - V_{C1} - V_{out} \\ V_{L2} = -V_{out} \end{aligned}\right\} \tag{14}$$

$$-V_{in} + V_{L1} + V_{C1} - V_{L2} = 0 \Rightarrow V_{C1} = V_{in} (\because \quad) \tag{15}$$

$$I_{C2} = I_D - I_{out} = I_D - \frac{V_{out}}{R_{load}} \tag{16}$$

$$V_{L1} = V_{in} - V_{C1} - V_{out} = 0 \Rightarrow V_{L1} = -V_{out} (\because \quad_{in}) \tag{17}$$

When the switch Q is ON and OFF, the inductors L_1 and L_2 voltages are equal to an instance $0 \le t \le DT$ and $DT \le t \le T$ as represented in Eq. (18). Further, the voltage output of the SEPIC converter is calculated from Eq. (19).

$$\left.\begin{aligned} V_{L1} = V_{in}, \quad 0 \le t \le DT \\ V_{L2} = -V_{out}, \quad DT \le t \le T \quad (\because \quad) \end{aligned}\right\} \tag{18}$$

$$V_{in}(DT) - V_{out}(1 - DT) = 0 \Rightarrow V_{out} = V_{in}\frac{DT}{1 - DT} \tag{19}$$

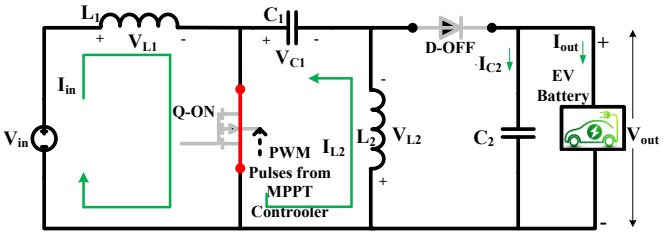

(a) Mode-1

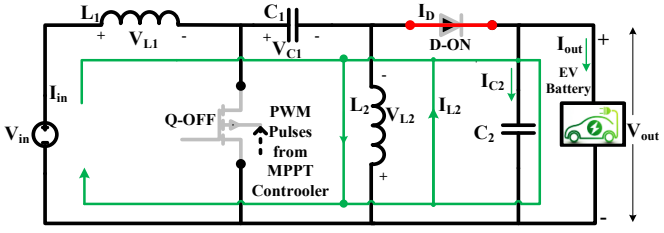

(b) Mode-2

Fig. 5. Current flow in the SEPIC converter during the switch ON and OFF states in various modes.

3.3. Solar Powered Buck-Boost Converter

This converter is a flexible DC-DC converter with a combination of both boost and buck converters for voltage conversion. The output voltage is regulated and maintained

constant based on the duty ratio of the converter switch [35]. The converter's switch is governed by the duty cycle (D), generated by the INC and P&O MPPT controllers to maintain the constant output voltage at the DC link.

- **Mode-1 (Switch Q is ON, 0 < t < DT):** The switch Q is turned ON, and the inductor L is charging with the supply current (I_{in}). In this mode, the diode D is forward-biased and acts as an open switch. The direction of current is represented in Fig. 6(a). The change in inductor current is derived as Eq. (20) and Eq. (21) during this operation.
- **Mode-2 (Switch Q is OFF, DT < t < T)**: In this mode of operation, the switch Q is turned OFF, and the diode D is turned ON. During this time, the inductor discharges the energy and transfers it to EV loads. The current flow direction is represented in Fig. 6(b), and the change in inductor current during the OFF state is calculated through Eq. (22) and Eq. (23). The output voltage of the converter under steady-state is derived as given in Eq. (24).

$$V_L = V_{in} = L\frac{dI_L}{dt} \tag{20}$$

$$\frac{V_{in}}{L} = \frac{dI_L}{dt} = \frac{\Delta I_L}{\Delta t} = \frac{\Delta I_L}{DT} \Rightarrow (\Delta I_L)_{closed} = \frac{V_{in}}{L} DT \tag{21}$$

$$V_L = V_{out} = L\frac{dI_L}{dt} \tag{22}$$

$$\left.\begin{aligned} \frac{V_{in}}{L} = \frac{dI_L}{dt} = \frac{\Delta I_L}{\Delta t} = \frac{\Delta I_L}{T(1-D)} \\ \Rightarrow \Delta I_L\big|_{open} = \frac{TV_{out}}{L}(1-D) \end{aligned}\right\} \tag{23}$$

$$\left.\begin{aligned} \Delta I_L\big|_{open} + \Delta I_L\big|_{closed} = 0 \Rightarrow \frac{V_{in}DT + V_{out}(1-D)T}{L} = 0 \\ \therefore V_{out} = -\frac{D}{(1-D)}(V_{in}) \end{aligned}\right\} \tag{24}$$

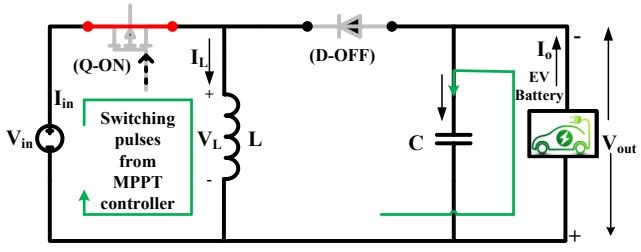

(a) Mode-1

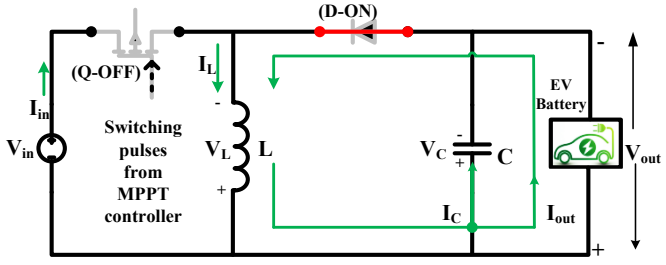

(b) Mode-2

Fig. 6. Current flow in the buck-boost converter during the switch ON and OFF states in various modes.

3.4. Solar Powered Zeta Converter

To manage the DC-DC conversion process efficiently, the zeta converter dynamically controls the voltage supplied to the EV battery [36]. This setup ensures the safe and effective charging of the EV battery. The voltage output is regulated and maintained constant based on the duty ratio of the converter switch, which is governed by the duty cycle (D), generated by the INC and P&O MPPT controllers.

- **Mode-1 (Switch Q is ON, 0 < t < DT):** The switch Q is turned ON, and diode D is turned OFF by reverse voltage. During this time interval (DT), both inductors L_i and L_o, and capacitor C_1 are charged. The current flow direction is denoted in Fig. 7(a). The change in inductor current and capacitor voltages is calculated from Eq. (25) to Eq. (26).
- **Mode-2 (Switch Q is OFF, DT < t < T)**: During this time interval ($DT < t < T$), the switch Q is turned OFF, and the diode D is turned ON and is in the forward-biased mode. Due to turning the switch OFF, both the inductors L_i and L_o are discharging into capacitors C_1 and C_D, respectively, as shown in Fig. 7(b). The inductor current and capacitor voltages are calculated from Eq. (27) to Eq. (28).

$$\left.\begin{aligned} V_{in} = V_{Li} \text{ and } \frac{dI_{Li}}{dt} = \frac{V_{in}}{L_i} \text{ and } \frac{dV_{Ci}}{dt} = -\frac{dI_{Lo}}{C_1} \end{aligned}\right\} \tag{25}$$

$$\left.\begin{aligned} \frac{dI_{Lo}}{dt} = \frac{V_{C1}}{L_o} + \frac{V_{in}}{L_o} - \frac{V_{Cd}}{L_o} \text{ and } \frac{dV_{Cd}}{dt} = \frac{I_{Lo}}{C_d} - \frac{V_{Cd}}{R_i C_d} \end{aligned}\right\} \tag{26}$$

$$\left.\begin{aligned} -\frac{V_{C1}}{L_i} = \frac{dI_{Li}}{dt} \text{ and } -\frac{I_{Li}}{C_1} = \frac{dV_{C1}}{dt} \end{aligned}\right\} \tag{27}$$

$$\left.\begin{aligned} -\frac{V_{Cd}}{L_o} = \frac{dI_{Lo}}{dt} \text{ and } \frac{I_{Lo}}{C_d} - \frac{V_{Cd}}{R_i \times C_d} = \frac{dV_{Cd}}{dt} \end{aligned}\right\} \tag{28}$$

The output voltage of the zeta converter is given as Eq. (29).

$$V_{out} = \frac{D}{1-D} V_{in} \tag{29}$$

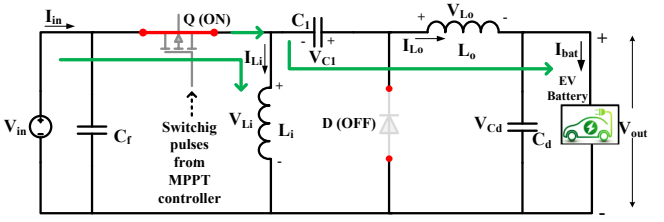

(a) Mode-1

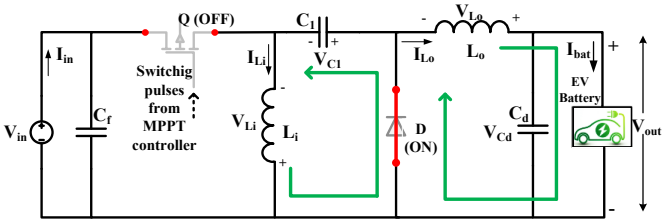

(b) Mode-2

Fig. 7. Current flow in the zeta converter during the switch ON and OFF states in various modes.

3.5. Solar Powered Flyback Converter

The flyback converter provides electrical isolation between solar panels and electric vehicles. The solar PV panels generate variable output voltages based on irradiation and temperature conditions. The flyback converter handles a wide range of input voltages and steps up or down the voltage as needed to recharge the EV batteries. The flyback converter topology is discussed in three modes of operation as follows [37].

- **Mode-1 (Switch Q is ON, 0 < t < DT):** The flyback transformer's primary is directly linked to the input voltage (V_{in}) source. Once the switch Q is ON at *DT,* the input current (I_{in}) flows to the primary. At this time, the input current and primary current (I_p) are the same as the magnetizing current (I_m). This causes an increase in primary current and magnetic flux, effectively storing energy in the flyback transformer. The induced voltage (V_p) in the secondary winding is negative, leading to the reverse biasing of the diode (*D-OFF*). At this time, the output capacitor efficiently supplies energy to the EVs as shown in Fig. 8(a). The flyback transformer secondary voltage (V_s), the change in magnetizing current in the flyback transformer primary winding (ΔI_{Lm}), and the flyback converter output voltage (V_{out}) are calculated using Eq. (30) and Eq. (31).
- **Mode-2 (Switch Q is OFF, DT < t < T)**: The stored energy in the flyback transformer winding does not immediately dissipate to zero when switch *Q* is turned OFF. During this time interval, the flyback transformer primary current (I_p) and magnetic flux decrease. The diode (*D*) allows current to flow from the flyback transformer according to Faraday's law of electromagnetic induction due to forward bias. The energy from the flyback transformer recharges the output capacitor and EV battery, as shown in Fig. 8(b). The diode current (I_D), capacitor current (I_{Cout}), and output current (I_{out}) are calculated as Eq. (32) and Eq. (33).
- **Mode-3 (Switch Q is ON)**: In this Mode-3, the already charged output capacitor (C_{out}) discharges the energy through the EVs. The high value of the output capacitor reduces the output ripples and maintains the constant output voltage (V_{out}) across the load terminals, irrespective of switching ON and OFF conditions to recharge the EV batteries represented in Fig. 8(c). The voltage output of the converter is calculated from Eq. (34) under steady-state conditions.

$$\left.\begin{aligned} V_{in} = V_p = L_m \frac{dI_{Lm}}{dt} = L_m \frac{\Delta I_{Lm}}{\Delta t} \\ (\Delta I_{Lm})_{closed} = \frac{V_{in}(DT)}{Lm} \end{aligned}\right\} \quad (30)$$

$$\left.\begin{aligned} V_s = V_p \frac{N_2}{N_1} = V_{in} \frac{N_2}{N_1} \\ V_D = -V_{out} - V_{in} \frac{N_2}{N_1} \Rightarrow V_{out} = -V_D - V_{in} \frac{N_2}{N_1} \end{aligned}\right\} \quad (31)$$

$$\left.\begin{aligned} V_p = -V_{out}\left(\frac{N_1}{N_2}\right) \\ V_s = -V_{out} \\ L_m\left(\frac{dI_{Lm}}{dt}\right) = V_p = -V_{out}\left(\frac{N_1}{N_2}\right) \end{aligned}\right\} \quad (32)$$

$$\left.\begin{aligned} L_m\left(\frac{dI_{Lm}}{dt}\right) = L_m\left(\frac{\Delta I_{Lm}}{\Delta t}\right) = \frac{\Delta I_{Lm}}{(1-D)T} = -\frac{V_{out}}{L_m}\left(\frac{N_1}{N_2}\right) \\ \left.\frac{\Delta I_{Lm}}{\Delta t}\right|_{open} = -\frac{V_{out}}{L_m}\left(\frac{N_1}{N_2}\right)(1-D)T \end{aligned}\right\} \quad (33)$$

$$\left.\begin{aligned} \Delta I_{Lm}|_{closed} + \Delta I_{Lm}|_{open} = 0 \\ V_{out} = \left(\frac{D}{1-D} \times \frac{N_1}{N_2}\right) V_{in} \end{aligned}\right\} \quad (34)$$

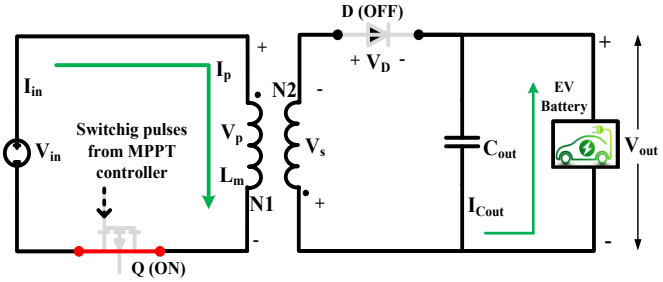

(a) Mode-1

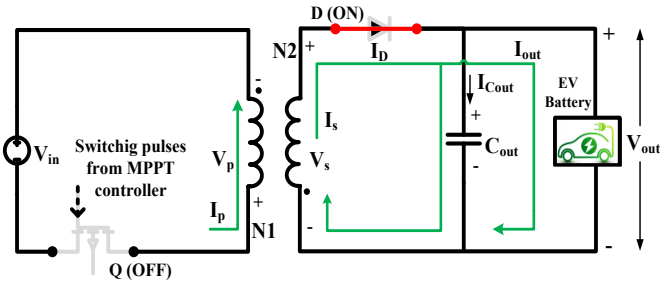

(b) Mode-2

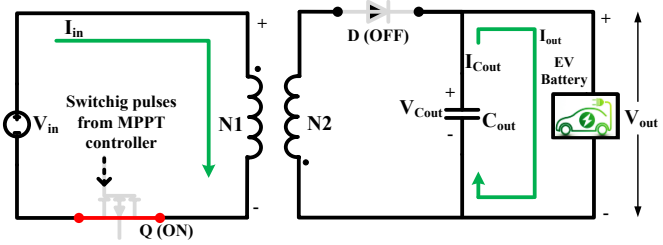

(c) Mode-3

Fig. 8. Current flow in the Flyback converter during the switch ON and OFF states in various modes.

4. MPPT Control of Solar-Powered Charging Stations

The implementation of a charge controller equipped with MPPT technology to efficiently harness the maximum power from photovoltaic panels. These MPPT algorithms are crucial for solar systems due to their ability to maximize energy output, enhance efficiency, adapt to changing environmental

conditions, accommodate various panel types, and optimize the performance of multi-panel setups [38, 39]. In this article, two MPPT algorithms are implemented as shown in Fig. 9 for extracting the maximum power from a solar system intended for an EV battery charge controller. The P&O and INC-based MPPT controllers [40, 41] are used in this paper to track maximum power from solar PV panels by integrating various DC-DC converters that are discussed in the previous section.

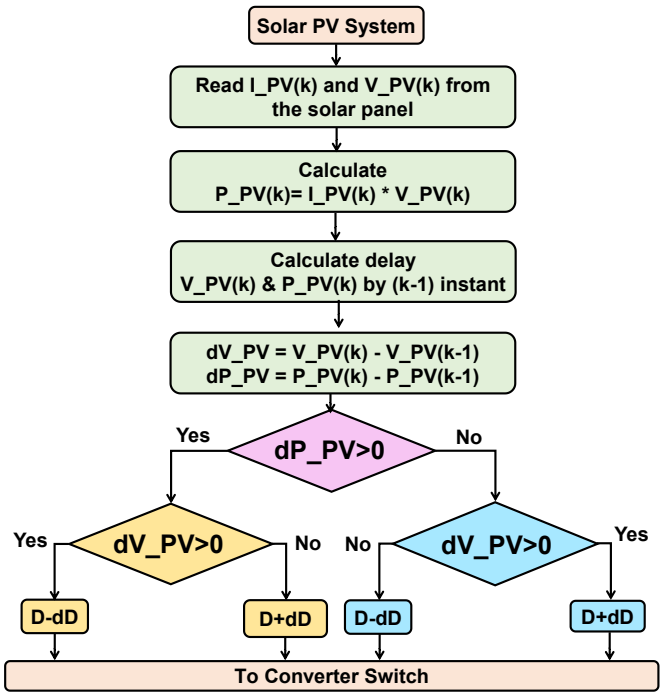

(a) P&O method

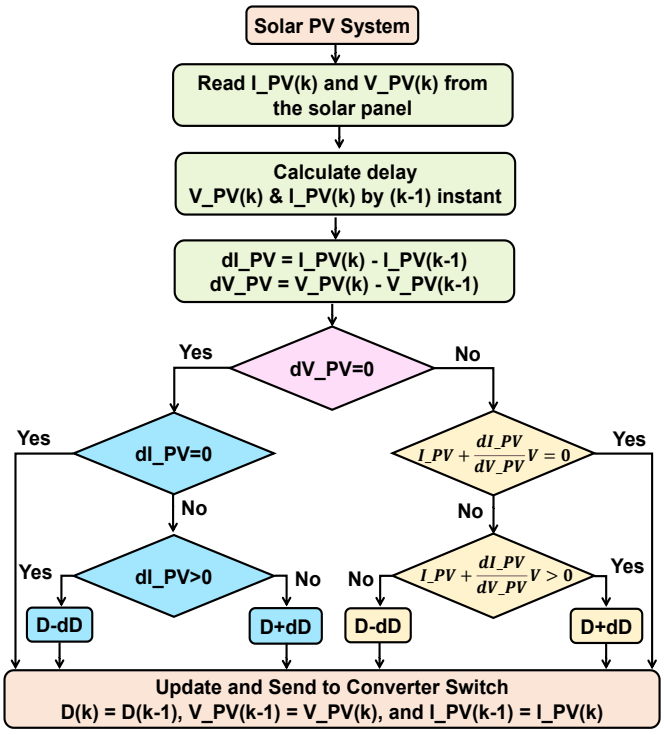

(b) INC method

Fig. 9. Flowcharts of various MPPT control methods.

4.1. P&O-Based MPPT Controller

The P&O MPPT method continuously perturbs the operation voltage (*V_PV(k)*) and currents (*I_PV(k)*) of a solar panel. This perturbation is followed by measuring the resulting power output (*P_PV(k)*). By comparing the newly measured power (*P_PV(k-1)*) with the previous value, the system determines the increased or decreased power from Eq. (35). This iterative process is designed to bring the system closer to the maximum power point and optimize energy production, as represented in the flowchart as shown in Fig. 9(a).

$$\left.\begin{aligned}\text{Increment of Power} &= \left[P\_PV(k)\right]+\left[P\_PV(k-1)\right]\\ \text{Decrement of Power} &= \left[P\_PV(k)\right]-\left[P\_PV(k-1)\right]\end{aligned}\right\} \quad (35)$$

4.2. INC-Based MPPT Controller

The incremental conductance MPPT controller is an advanced tracking technique used in this solar charging station to optimize power output from solar panels by adjusting the operating point [42, 43]. The INC method continually assesses the relationship between incremental changes in power and voltage or current to accurately track the maximum power point. This method starts with an initial MPP estimate and then calculates incremental changes in power and current/ voltage (*dI_PV/dV_PV*) and compares with reference values (*I_PV*). Based on continuous adjustments and comparisons, this method tracks the maximum power from solar panels. The implementation of the INC method is explained step by step in the flowchart, and it is represented in Fig. 9(b).

5. Results and Discussions

The results provide the performance characteristics and their comparative analysis of the considered five key DC-DC converter circuits, namely Buck-Boost, SEPIC, Cuk, Zeta, and Flyback. Their performance is assessed based on their ability to produce the maximum power from the solar PV system, their ability to keep constant voltage at the converter's output terminals, and their ability to obtain the maximum efficiency from the converters. To test the performance of these converters, different possible test cases are implemented as shown in Table 1 with various combinations of irradiance, temperature, and EV battery SOC.

Table 1. Test cases to compare the converter performance

Case	Irradiance	Temperature	Battery SOC (%)
1	High (1000 W/m^2)	High (40 °C)	70 (High)
2	Low (500 W/m^2)	Low (25 °C)	70 (High)
3	High (1000 W/m^2)	High (40 °C)	30 (Low)
4	Low (500 W/m^2)	Low (25 °C)	30 (Low)

Various results, namely solar PV power characteristics, voltage characteristics, and efficiency characteristics of converters with P&O and INC MPPT controllers, are plotted and compared. The comparative analysis under these test cases is presented in the following subsections.

5.1. Analysis of Results Obtained Under Test Case-1

In this test case-1, both the solar irradiance and temperature are high for a period of 0.5 secs. The MPPT controllers, like P&O and the INC, are implemented to extract the maximum power from the solar panels to recharge the batteries. In this case-1, only 70% SOC of the EV battery is connected to investigate various DC-DC converters using P&O and INC MPPT controllers. Figure 10 represents the maximum power obtained from the solar panels. Figures 11 and 12 show the converter's output voltages and efficiency, respectively, using the P&O MPPT controller. For high irradiation and temperature conditions, the maximum power produced from the flyback converter is 1588.9 W, the buck-boost converter is 1582.5 W, the ZETA converter is 1577.5 W, the CUK converter is 1577.5 W, and the SEPIC converter is 1577.5 W. All the converters maintain the DC link voltage around 216.57 V. The efficiency of ZETA converters is 97.3%, and both the flyback and buck-boost converters are 97.2%. The efficiency obtained from the SEPIC and CUK converters is 97.1% and 97%, respectively. From these results, by considering all three responses (efficiency, solar power, and DC link voltage) at steady state during 0.4-0.44 sec, more ripple content and oscillations are seen from all the converters except the flyback converter.

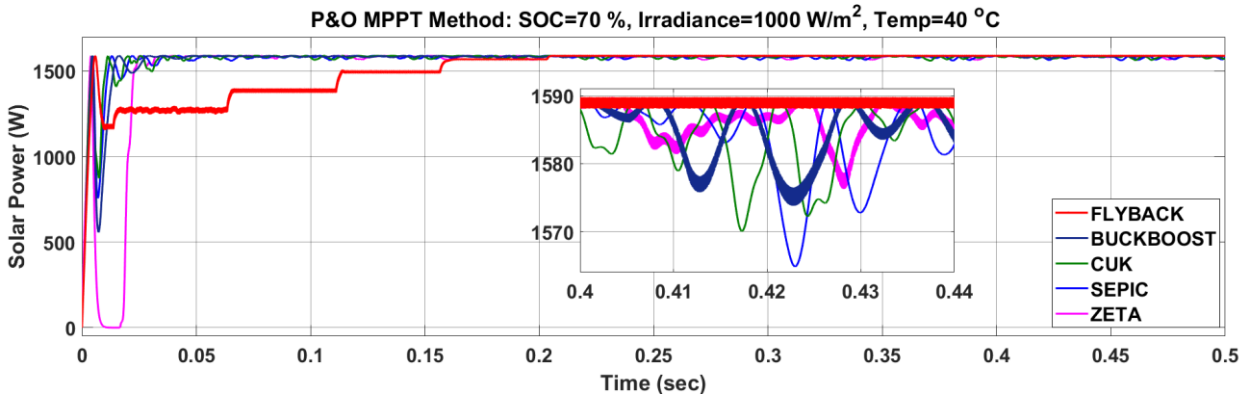

Fig. 10. Assessment of different DC-DC converters in terms of solar power extraction using P&O MPPT controller.

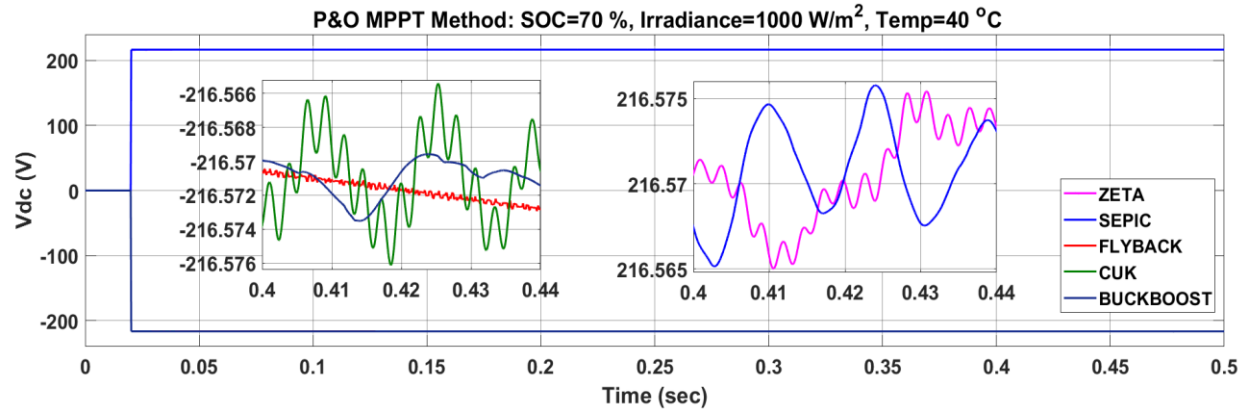

Fig. 11. Assessment of different DC-DC converters in terms of output voltage using P&O MPPT controller.

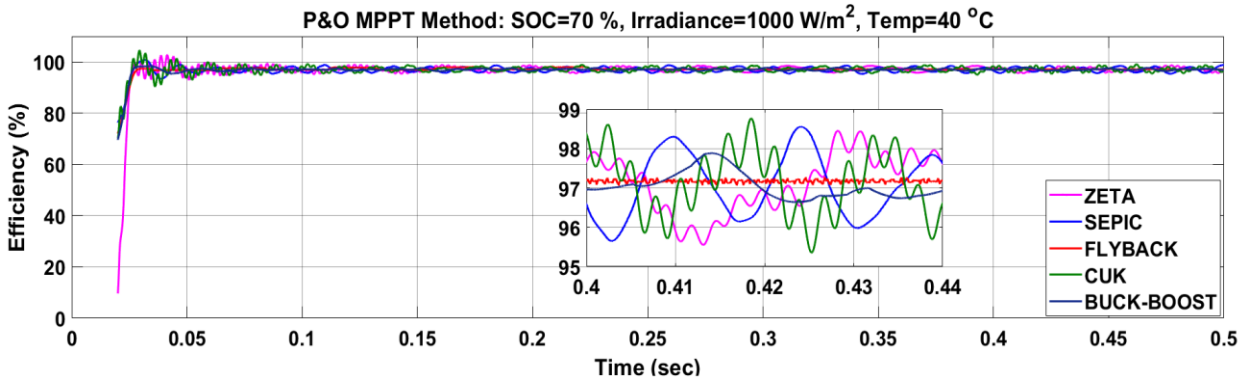

Fig. 12. Assessment of different DC-DC converters in terms of efficiency using P&O MPPT controller.

The maximum solar power extraction, converter's output voltage, and efficiency using the INC MPPT controller are shown in Fig. 13, Fig. 14, and Fig. 15, respectively. With the higher value of irradiation and temperature, the maximum power extracted from the flyback converter is 1588.9 W, the buck-boost converter is 1586 W, the Zeta converter is 1581 W, the Cuk converter is 1578 W, and the SEPIC converter is 1576.5 W. It is also seen that all DC-DC converters retain the constant DC link voltage of 216.5 V. The efficiency obtained from the buck-boost converters is 97.53%, and the zeta and flyback converters are 97.52% and 97.17%. The lowest efficiency obtained is from the SEPIC and Cuk converters of 97.02% and 96.95%, respectively. From the results, by considering all three waveforms at steady state during 0.4-0.44 sec, more ripple content and oscillations are observed from all the converters except the flyback converter.

The overall quantitative analysis of test case-1 is consolidated in Table 2. From this, it is concluded that the performance of the flyback converter is superior to that of the other conventional converters in the context of maximum power extraction. Better efficiency is obtained from the zeta converter with a P&O MPPT controller and a buck-boost converter with an INC MPPT controller. Also, all solar-powered DC-DC converters maintain a constant output voltage.

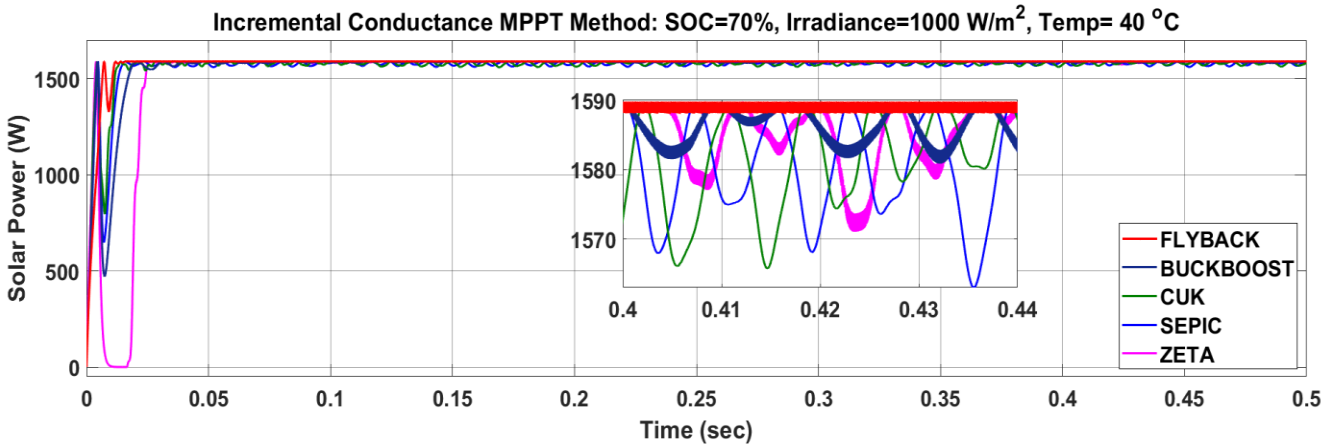

Fig. 13. Assessment of different DC-DC converters in terms of solar power extraction using the INC MPPT controller.

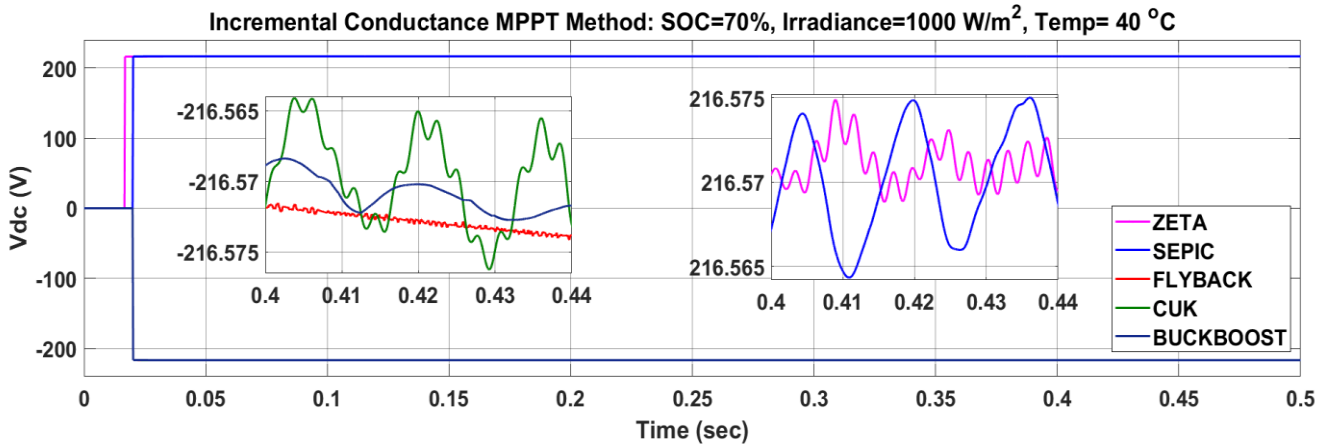

Fig. 14. Assessment of different DC-DC converters in terms of output voltage using the INC MPPT controller.

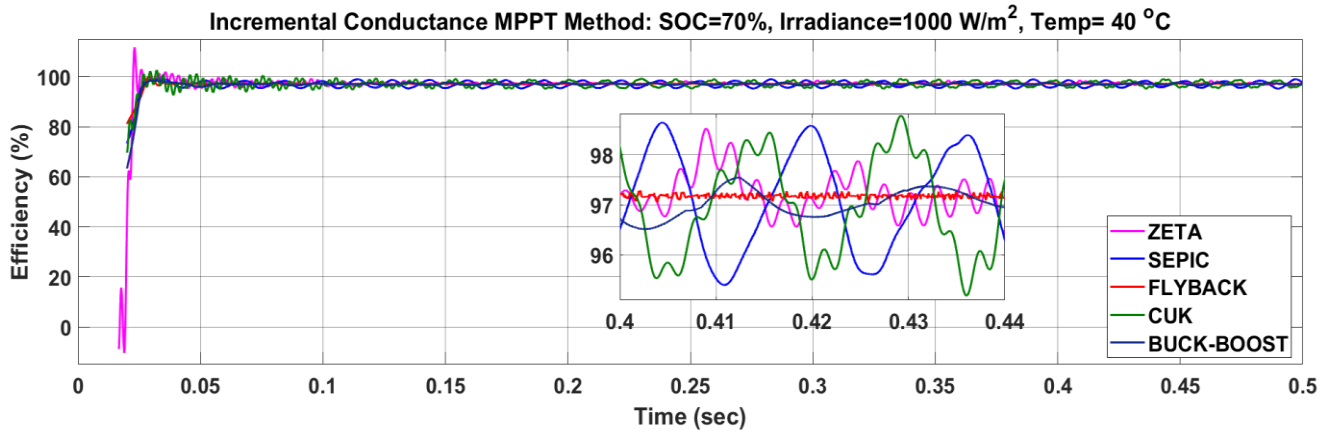

Fig. 15. Assessment of different DC-DC converters in terms of efficiency using the INC MPPT controller.

Table 2. Performance comparison of converters with respect to test case-1

Converter	Solar Power (P_{pv} in W)		DC Link Voltage (V_{dc} in V)		Efficiency (%)	
	P&O	INC	P&O	INC	P&O	INC
ZETA	1577.5	1581.0	217	217	97.3	97.52
SEPIC	1577.5	1576.5	217	217	97.1	97.02
FLYBACK	1588.9	1588.9	-217	-217	97.2	97.17
CUK	1577.5	1578.0	-217	-217	97.0	96.95
BUCK-BOOST	1582.5	1586.0	-217	-217	97.2	97.53
Superior	FLYBACK	FLYBACK	All Converters	All Converters	ZETA	BUCK-BOOST

5.2. Analysis of Results Obtained Under Test Case-2

In test case-2, both the solar irradiance (500 W/m^2) and temperature (25 ˚C) are low for a period of 0.5 secs. The P&O and INC MPPT controllers are implemented to extract the maximum power from the solar panels. In this test case-2, only 70% SOC of the EV battery is connected to investigate various DC-DC converters using P&O and INC MPPT controllers. Figure 16 represents the maximum power obtained from the solar panels. Figures 17 and 18 show the converter's output voltages and efficiency, respectively, using the P&O MPPT controller. For lower irradiation and temperature conditions, the maximum power produced from the flyback converter is 866.9 W, the ZETA converter is 859.7 W, the CUK converter is 857 W, the SEPIC converter is 855 W, and the buck-boost converter is 854.5 W. All investigated converters maintain the DC link voltage around 216.4 V. The efficiency of flyback converters is 97%, and ZETA, buck-boost, and SEPIC converters are 94.5%. The efficiency obtained from the CUK converter is 94% compared with other converters.

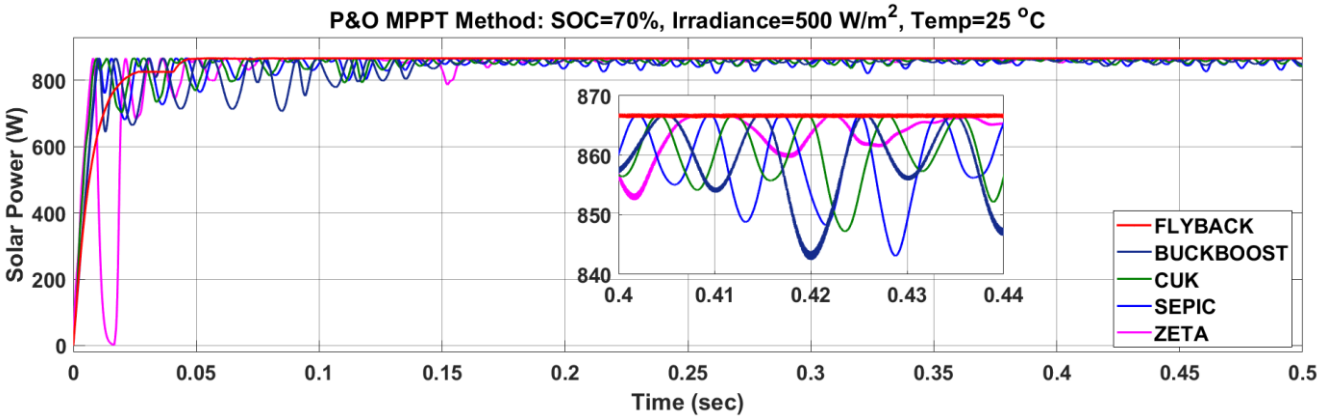

Fig. 16. Assessment of different DC-DC converters in terms of solar power extraction using P&O MPPT controller.

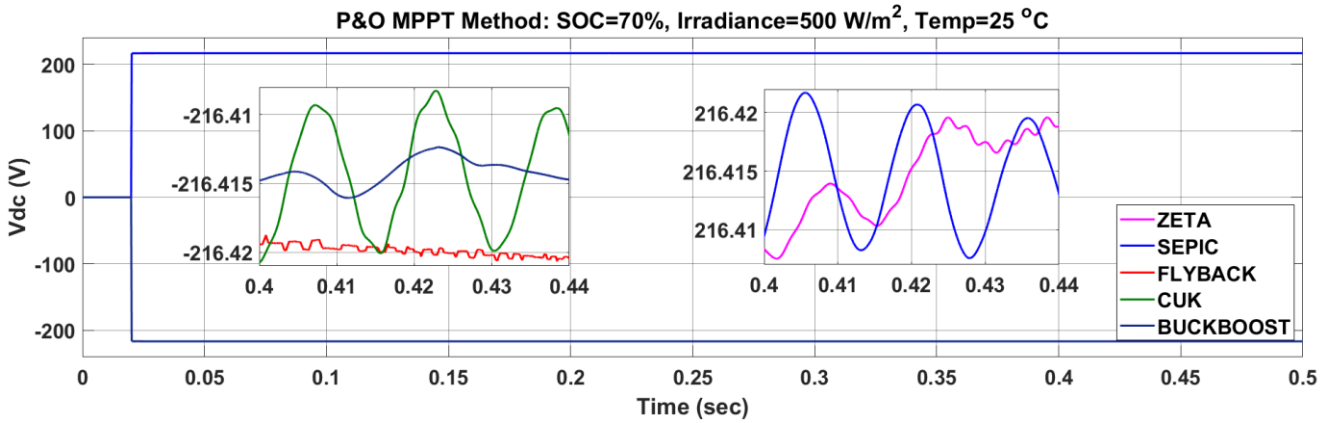

Fig. 17. Assessment of different DC-DC converters in terms of output voltage using P&O controller.

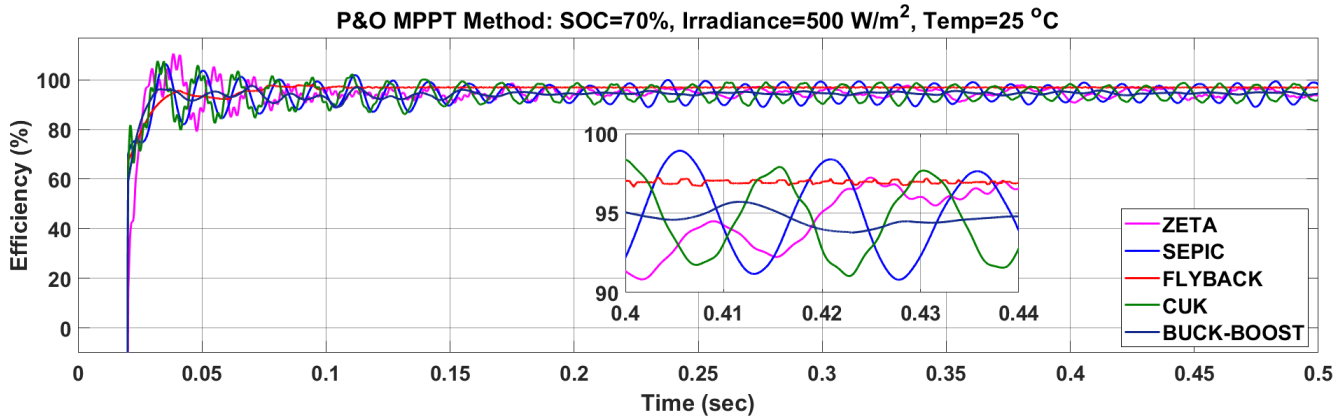

Fig. 18. Assessment of different DC-DC converters in terms of efficiency using P&O MPPT controller.

By considering all three waveforms at steady state during 0.4-0.44 sec, more ripple content and oscillations are observed from all the converters except the flyback converter. The maximum power obtained from the solar panels is depicted in Fig. 19. Figures 20 and 21 represent the converter's output voltages and efficiency, respectively, using an INC MPPT controller. With the lower value of irradiation and temperature conditions, the maximum power extracted from the flyback converter is 888.6 W, the ZETA converter is 863 W, the buck-boost converter is 856 W, the CUK converter is 851.5W, and the SEPIC converter is 842 W. In this test case-2, all DC-DC converters maintained a DC link voltage of around 216.4 V by investigation. The maximum efficiency obtained from the flyback converters is 96.76%, and both ZETA and buck-boost converters' efficiencies are 94.8%. The lowest efficiency obtained from the SEPIC converters is 94.25% compared with the other converters.

The overall quantitative analysis of test case-2 is summarized in Table 3. From this, it can be concluded that the performance of the flyback converter is superior to that of the other converters in the context of maximum power extraction and efficiency. Besides, all solar-powered DC-DC converters provide a constant output voltage.

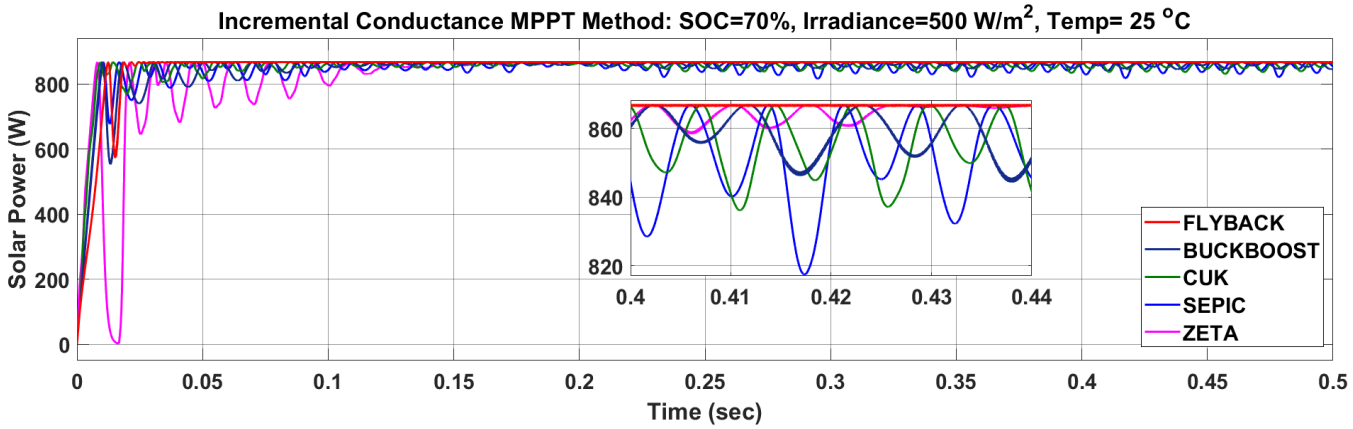

Fig. 19. Assessment of different DC-DC converters in terms of solar power extraction using the INC MPPT controller.

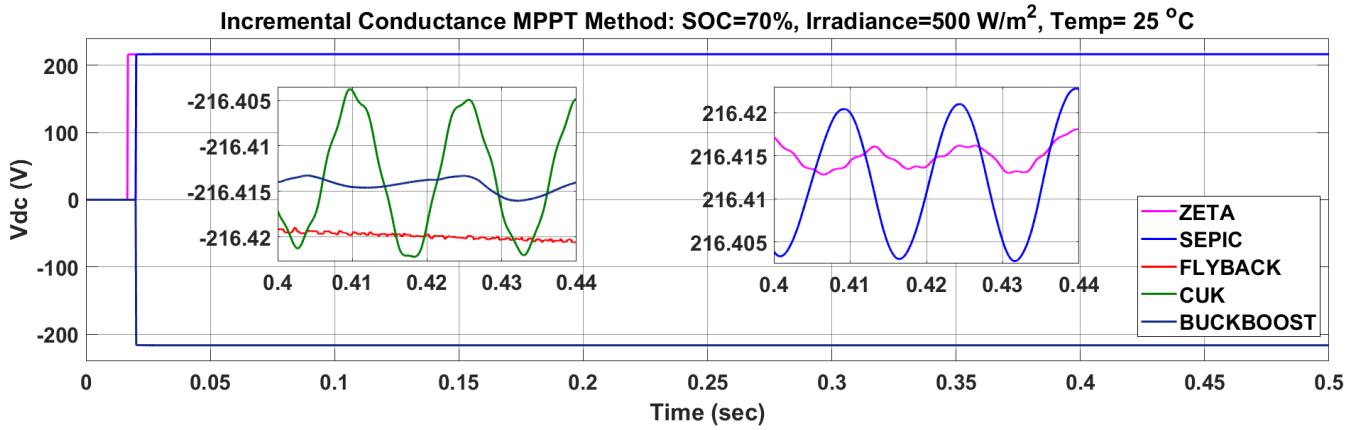

Fig. 20. Assessment of different DC-DC converters in terms of output voltage using the INC MPPT controller.

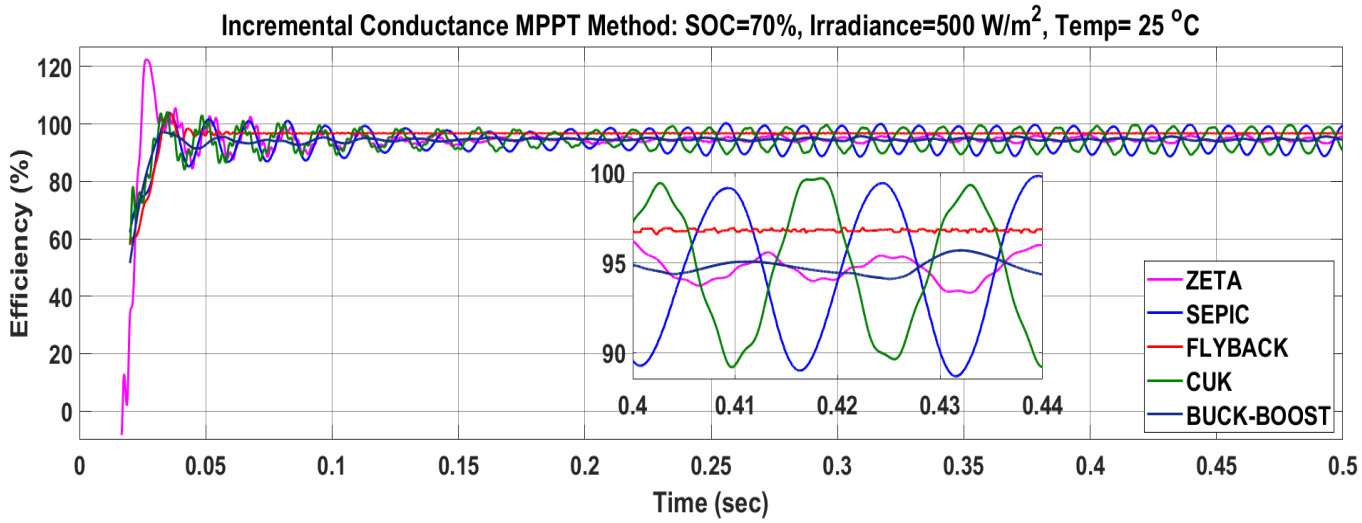

Fig. 21. Assessment of different DC-DC converters in terms of efficiency using the INC MPPT controller.

Table 3. Performance comparison of converters with respect to test case-2

Converter	Solar Power (P_{pv} in W)		DC Link Voltage (V_{dc} in V)		Efficiency (%)	
	P&O	INC	P&O	INC	P&O	INC
ZETA	859.7	863.0	217	217	94.5	94.80
SEPIC	855.0	842.0	217	217	94.5	94.25
FLYBACK	866.9	866.6	-217	-217	97.0	96.76
CUK	857.0	851.5	-217	-217	94.0	94.35
BUCK-BOOST	854.5	856.0	-217	-217	94.5	94.80
Superior	FLYBACK	FLYBACK	All Converters	All Converters	FLYBACK	FLYBACK

5.3. Analysis of Results Obtained Under Test Case-3

In test case-3, both the solar irradiance (1000 W/m^2) and temperature (40 °C) are high for a period of 0.5 secs. The P&O and INC MPPT controllers are implemented to extract the maximum power from the solar panels. In this case, only 30% SOC of the EV battery is connected to investigate various DC-DC converters using P&O/INC MPPT methods. Figure 22 represents the maximum power obtained from the solar panels. Figures 23 and 24 show the converter's output voltages and efficiency, respectively, using a P&O MPPT controller. For higher irradiation and temperature conditions, the maximum power extracted from the flyback converter is 1588.1 W, the buck-boost converter is 1585 W, the Zeta converter is 1576 W, the Cuk converter is 1569.5 W, and the SEPIC converter is 1568W. All converters maintained the DC link voltage around 214 V. The efficiency of flyback converters is 97.57%, and CUK, ZETA, and SEPIC converters are 97.5%, 97.2%, and 97.15%, respectively. The efficiency obtained from the buck-boost converter is 96.92%.

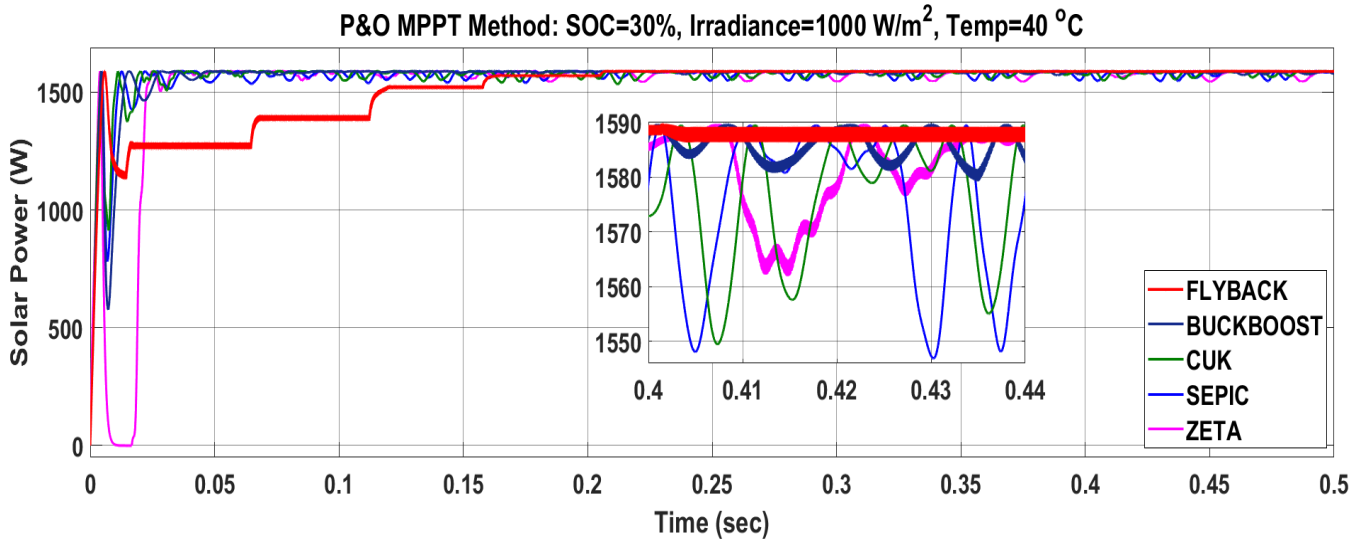

Fig. 22. Assessment of different DC-DC converters in terms of solar power extraction using P&O MPPT controller.

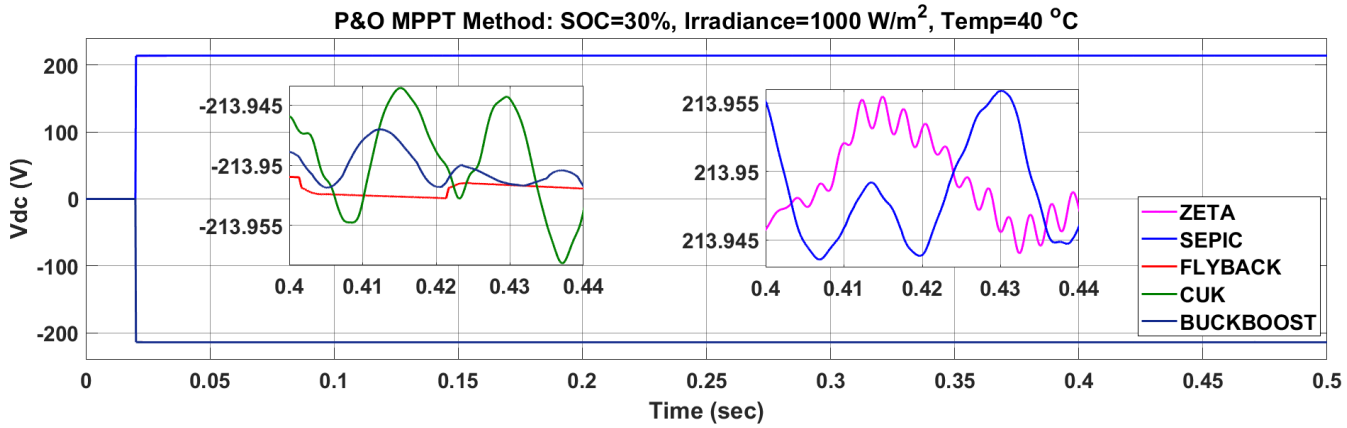

Fig. 23. Assessment of different DC-DC converters in terms of output voltage using P&O MPPT controller.

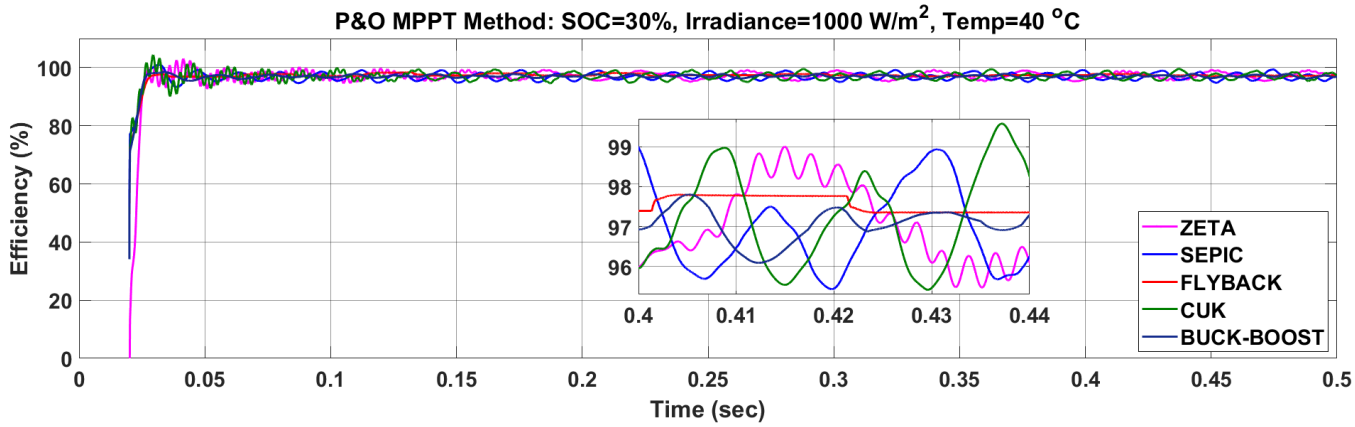

Fig. 24. Assessment of different DC-DC converters in terms of efficiency using P&O MPPT controller.

From the results, by considering all three waveforms at steady state during 0.4 sec to 0.44 sec, more ripple content and oscillations are observed from all the converters except the flyback converter. The maximum power obtained from the solar panels is depicted in Fig. 25, Fig. 26, and Fig. 27, which represent the converter's output voltages and efficiency, respectively, using an INC MPPT controller at 30% SOC. With the higher value of irradiation and temperature conditions, the maximum power produced from the flyback converter is 1588.9 W, the buck-boost converter is 1582.2 W, the ZETA converter is 1579.5 W, the SEPIC converter is 1569 W, and the CUK converter is 1562.5 W. In this test case-3, all DC-DC converters maintained a DC link voltage of around 216.4 V by investigation. The maximum efficiency obtained from the ZETA converters is 97.35%, the FC converter is 97.13%, SEPIC converter is 97.1%. The lowest efficiency obtained from buck-boost and CUK converters are 97.06 and 97%, respectively, compared with other converters.

The overall quantitative analysis of test case-3 is summarized in Table 4. From this, it is concluded that the performance of the flyback converter is superior to that of the other conventional converters in the context of maximum power extraction. Better efficiency was obtained from the flyback converter with P&O MPPT controller and zeta converter with INC MPPT controller, and all solar-powered DC-DC converters maintained a constant output voltage.

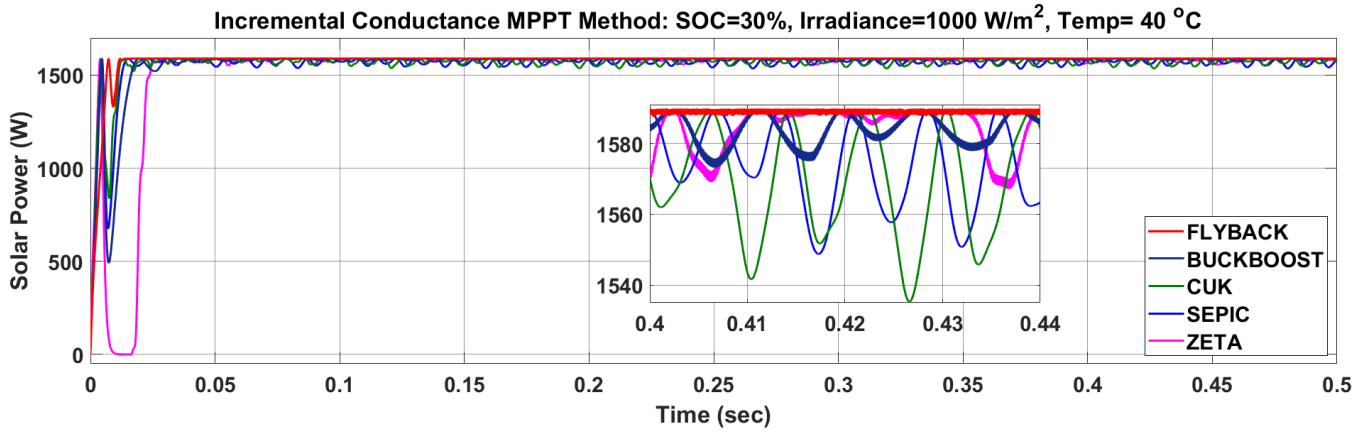

Fig. 25. Assessment of different DC-DC converters in terms of solar power extraction using the INC MPPT controller.

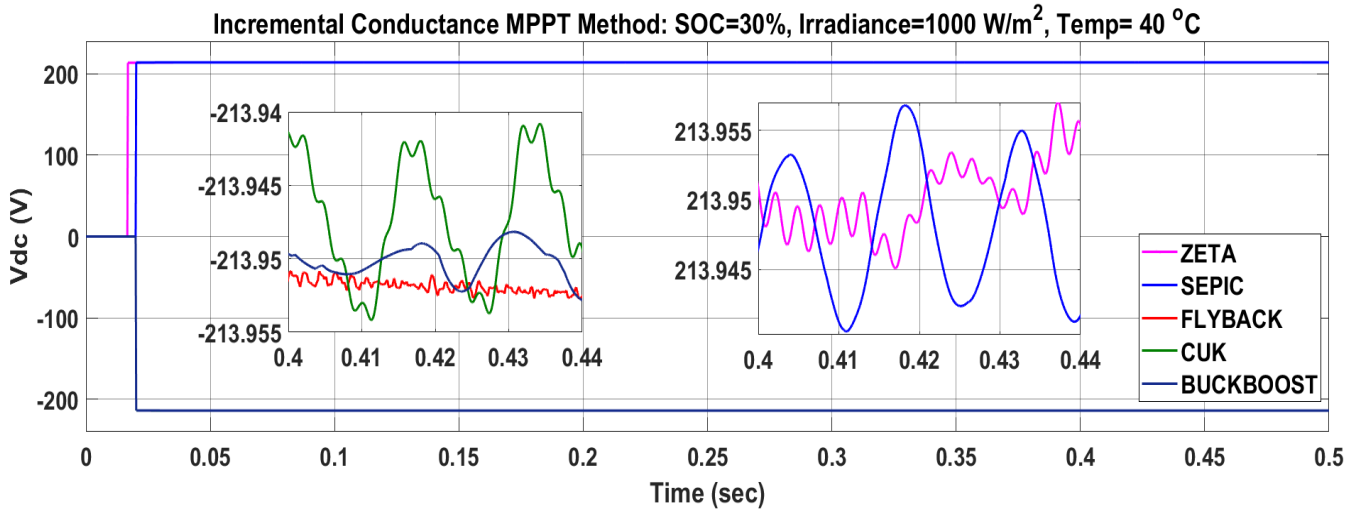

Fig. 26. Assessment of different DC-DC converters in terms of output voltage using the INC MPPT controller.

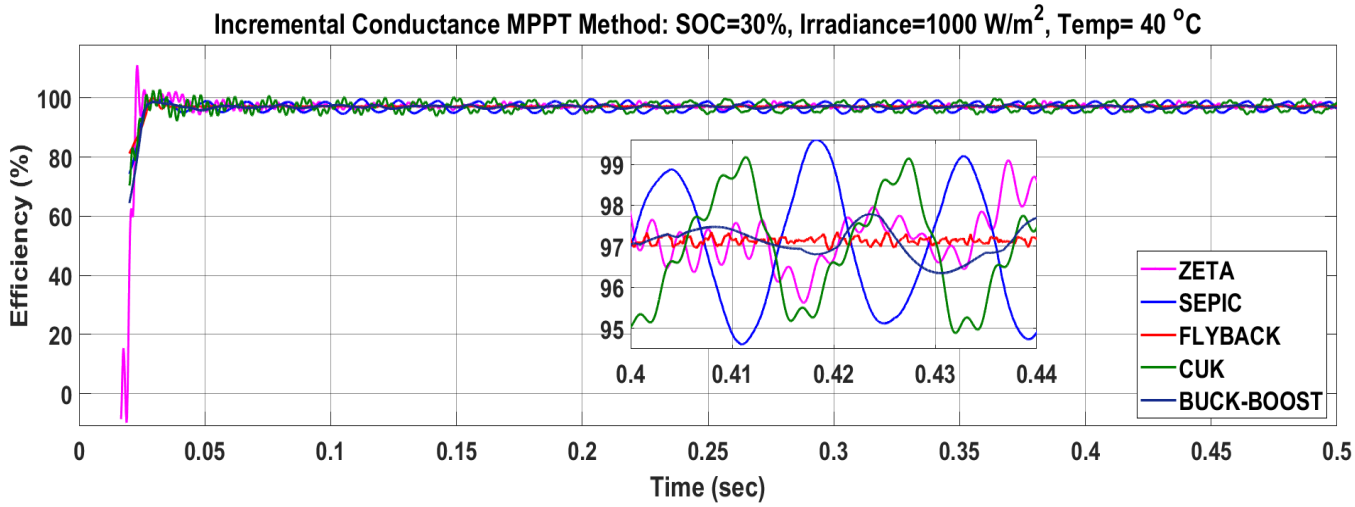

Fig. 27. Assessment of different DC-DC converters in terms of efficiency using the INC MPPT controller.

Table 4. Performance comparison of converters with respect to test case-3

Converter	Solar Power (P_{pv} in W)		DC Link Voltage (V_{dc} in V)		Efficiency (%)	
	P&O	INC	P&O	INC	P&O	INC
ZETA	1576.0	1579.5	214	214	97.20	97.35
SEPIC	1568.0	1569.0	214	214	97.15	97.10
FLYBACK	1588.1	1588.9	-214	-214	97.57	97.13
CUK	1569.5	1562.5	-214	-214	97.50	97.00
BUCK-BOOST	1585.0	1582.2	-214	-214	96.92	97.06
Superior	FLYBACK	FLYBACK	All Converters	All Converters	FLYBACK	ZETA

5.4. Analysis of Results Obtained Under Test Case-4

In this test case-4, both the solar temperature and irradiance are low for a period of 0.5 secs. The P&O and INC MPPT controllers are implemented to extract the maximum power from the solar panels. In this test case-4, only 30% SOC of the EV battery is connected to investigate various DC-DC converters using P&O and INC MPPT controllers. Figure 28 represents the maximum power obtained from the solar panels. Figures 29 and 30 show the converter's output voltages and efficiency, respectively, using a P&O MPPT controller. For lower irradiation and temperature conditions, the maximum power extracted from the flyback converter is 866.5 W, from the ZETA and buck-boost converters is 854.5 W, the SEPIC converter extracted 849 W, and the CUK converter is 845 W. All investigated converters maintain the DC link voltage around 214 V. The efficiency of the flyback converter is 96.97%, the buck-boost and SEPIC converters is 94.6%. The efficiency obtained from both ZETA and CUK converters is 94.4%.

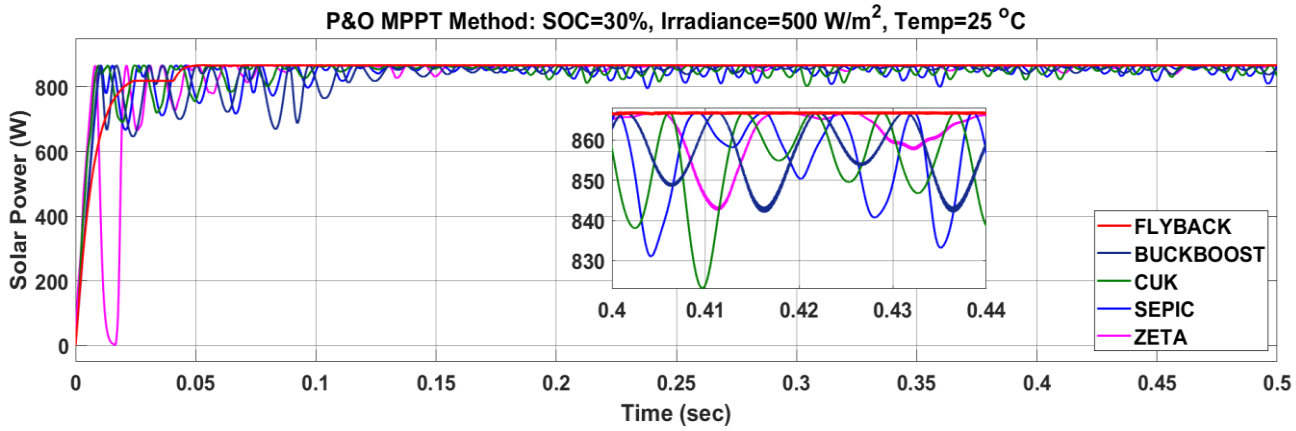

Fig. 28. Assessment of different DC-DC converters in terms of solar power extraction using P&O MPPT controller.

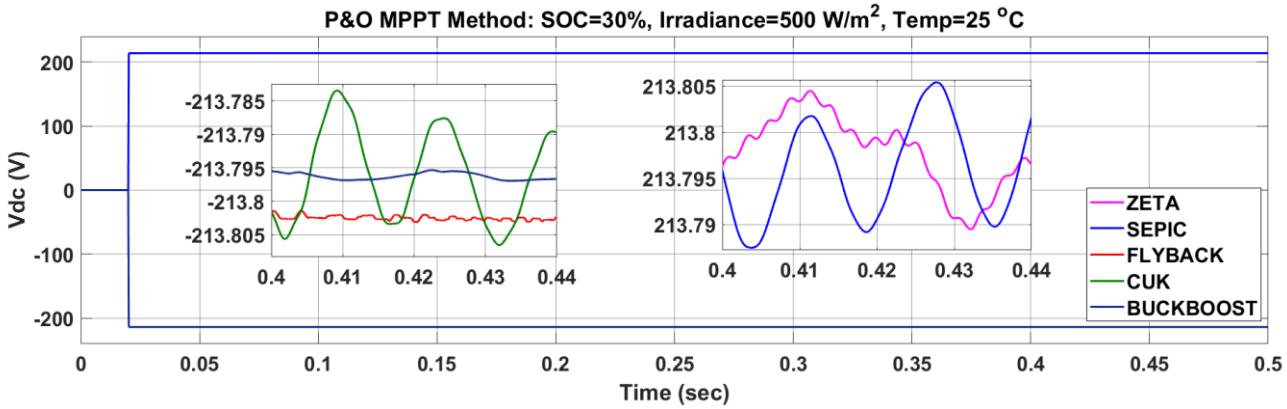

Fig. 29. Assessment of different DC-DC converters in terms of output voltage using P&O MPPT controller.

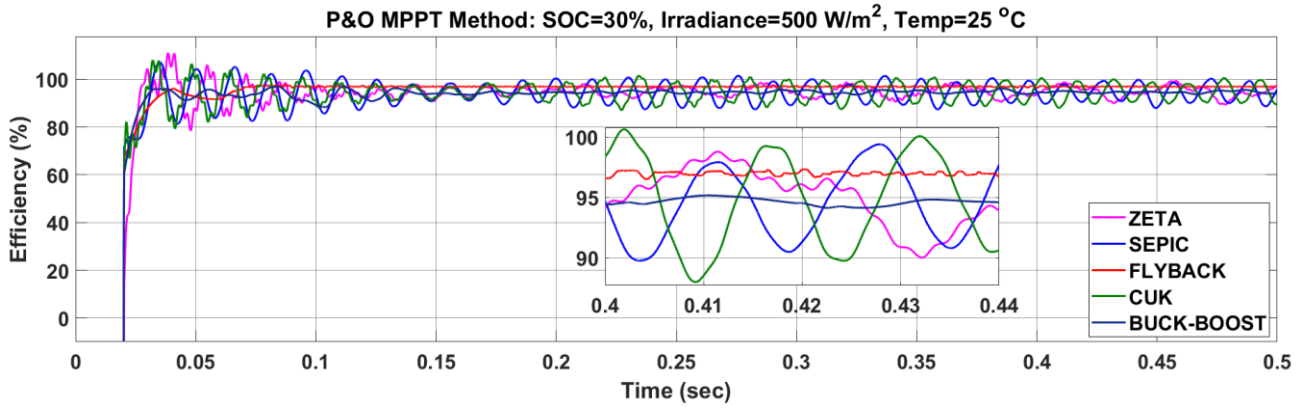

Fig. 30. Assessment of different DC-DC converters in terms of efficiency using P&O MPPT controller.

From the results, by considering all three waveforms at steady state during 0.4 sec to 0.44 sec, more ripple content and oscillations are observed from all the converters except the flyback converter. The maximum power obtained from the solar panels is depicted in Fig. 31. Figures 32 and 33 represent the converter's output voltages and efficiency, respectively, using an INC MPPT controller. With the lower value of irradiation and temperature conditions, the maximum power extracted from the flyback converter is 888.6 W, the ZETA converter is 857.5 W, the buck-boost converter is 851.5 W, both CUK and SEPIC converters extracted 837.5 W and 827 W, respectively. In this test case-4, all DC-DC converters maintained a voltage at the DC link around 214 V by investigation. The maximum efficiency obtained from the flyback converters is 96.8%, both ZETA and buck-boost converters are 94.8%, and the SEPIC converter is 94.1%. The lowest efficiency obtained from the CUK converters is 93.7% compared with other converters. The overall quantitative analysis of test case-4 is summarized in Table 5. From this, it is concluded that the performance of the flyback converter is superior to that of the other converters in the context of maximum power extraction and efficiency. Further, all solar-powered DC-DC converters maintained a constant output voltage.

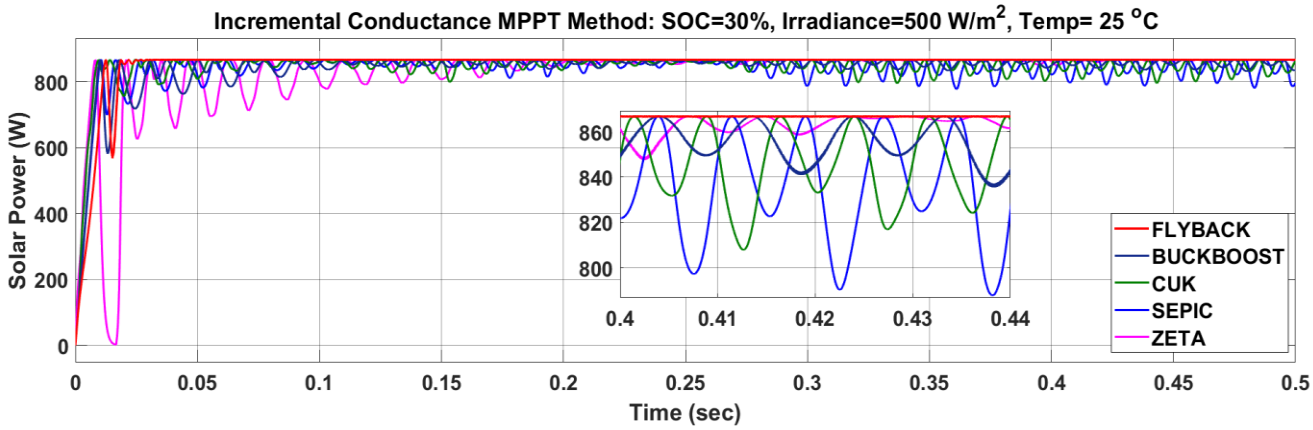

Fig. 31. Assessment of different DC-DC converters in terms of solar power extraction using the INC MPPT controller.

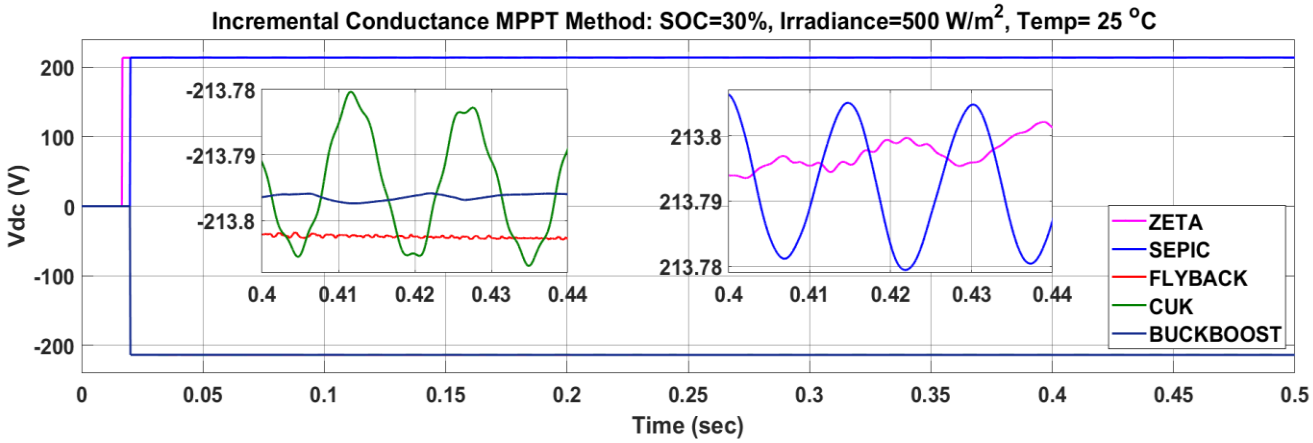

Fig. 32. Assessment of different DC-DC converters in terms of output voltage using the INC MPPT controller.

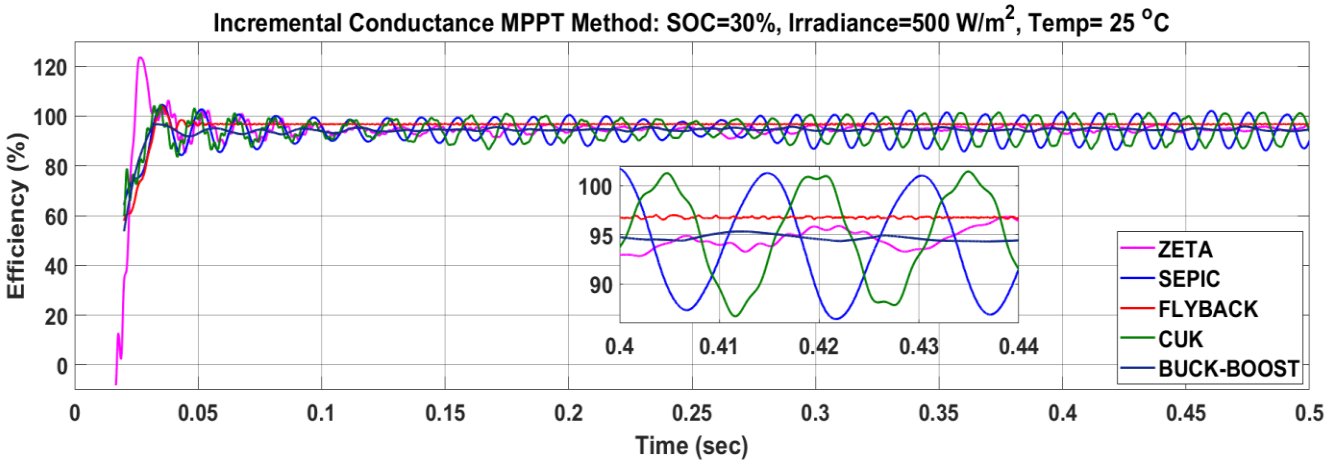

Fig. 33. Assessment of different DC-DC converters in terms of efficiency using the INC MPPT controller.

Table 5. Performance comparison of converters with respect to test case-4.

Converter	Solar Power (P_{pv} in W)		DC Link Voltage (V_{dc} in V)		Efficiency (%)	
	P&O	INC	P&O	INC	P&O	INC
ZETA	854.5	857.5	213.8	213.8	94.4	94.8
SEPIC	849.0	827.0	213.8	213.8	94.6	94.1
FLYBACK	866.5	866.6	-213.8	-213.8	96.9	96.8
CUK	845.0	837.5	-213.8	-213.8	94.4	93.7
BUCK-BOOST	854.5	851.5	-213.8	-213.8	94.6	94.8
Superior	FLYBACK	FLYBACK	All Converters	All Converters	FLYBACK	FLYBACK

6. Conclusions

This research conducts a comprehensive analysis aimed at exploring the ramifications of employing highly efficient DC-DC converters in solar PV systems to achieve optimal power tracking in solar-powered EV charging stations. Five DC-DC converters are implemented, namely Buck-Boost, SEPIC, Cuk, Zeta, and Flyback, along with two MPPT control mechanisms, namely P&O and INC. The performance is validated by executing various real-time test cases. The comparison is done by calculating various performance parameters, namely solar power, converter output voltage, and converter efficiency. All the salient findings of this work are summarized as follows.

- ***Solar Power Extraction***: Table 6 and Fig. 34 provide summarized findings with respect to the solar power extraction capability of various DC-DC converters. From these cumulative comparison results, it is found that the flyback converter is superior to other DC-DC converters in maximum solar power extraction ability in all test cases.
- ***Efficiency***: Table 7 and Fig. 35 provide summarized findings with respect to converter efficiency. From the cumulative comparison results, it is found that the flyback converter is superior to other DC-DC converters with respect to efficiency in most of the test cases.
- ***Converter Output Voltage***: The results indicate consistent maintenance of an optimal voltage level of around 216 V across various test cases for all converters. This underscores their ability to provide effective voltage regulation, particularly advantageous for electric vehicle charging applications.

Hence, based on the findings derived from various test cases, it is established that the solar charging station utilizing the flyback converter has surpassed the performance of the buck-boost, SEPIC, Cuk, and Zeta converter solar charging stations. This analysis indicates that the flyback converter stands out as the most effective choice for EV applications.

Table 6. Cumulative quantitative performance comparison with respect to solar power extraction

Converter Type	P&O MPPT Controller				INC MPPT Controller			
Test Cases	**1**	**2**	**3**	**4**	**1**	**2**	**3**	**4**
ZETA	1577.5	859.7	1576.0	854.5	1581.0	863.0	1579.5	857.5
SEPIC	1577.5	855.0	1568.0	849.0	1576.5	842.0	1569.0	827.0
FLYBACK	**1588.9**	**866.9**	**1588.1**	**866.5**	**1588.9**	**866.6**	**1588.9**	**866.6**
CUK	1577.5	857.0	1569.5	845.0	1578.0	851.5	1562.5	837.5
BUCK-BOOST	1582.5	854.5	1585.0	854.5	1586.0	856.0	1582.2	851.5

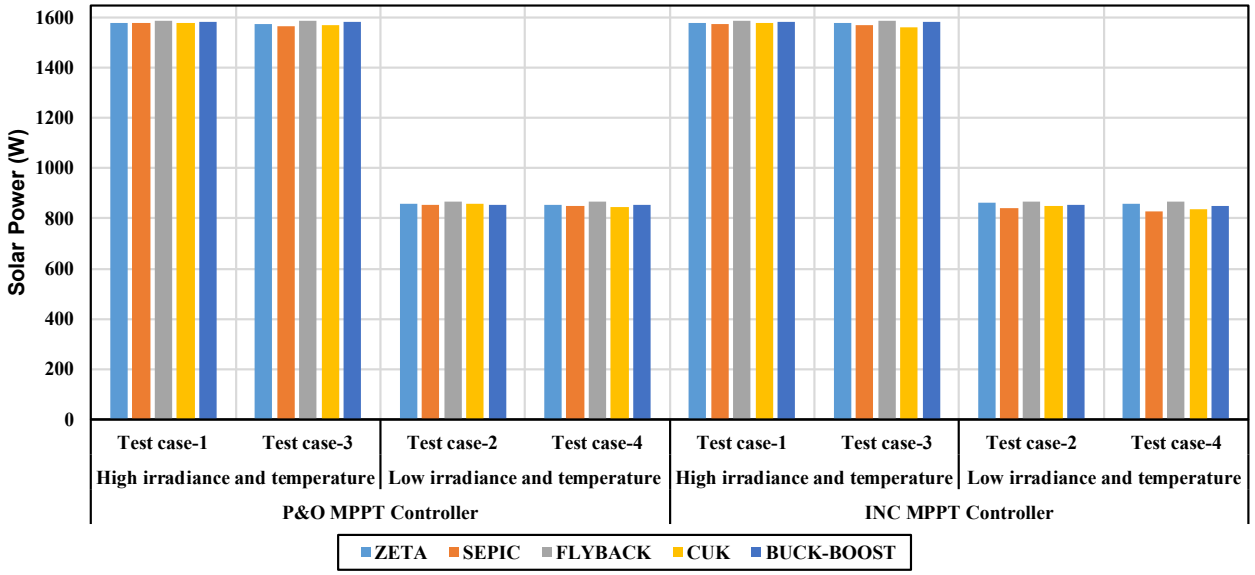

Fig. 34. Cumulative performance comparison of various converters with respect to solar power extraction.

Table 7. Cumulative quantitative performance comparison with respect to efficiency

Converter Type	P&O MPPT Controller				INC MPPT Controller			
Test Cases	**1**	**2**	**3**	**4**	**1**	**2**	**3**	**4**
ZETA	**97.3**	94.5	97.20	94.4	97.52	94.80	**97.35**	94.8
SEPIC	97.1	94.5	97.15	94.6	97.02	94.25	97.10	94.1
FLYBACK	97.2	**97.0**	**97.57**	**96.9**	97.17	**96.76**	97.13	**96.8**
CUK	97.0	94.0	97.50	94.4	96.95	94.35	97.00	93.7
BUCK-BOOST	97.2	94.5	96.92	94.6	**97.53**	94.80	97.06	94.8

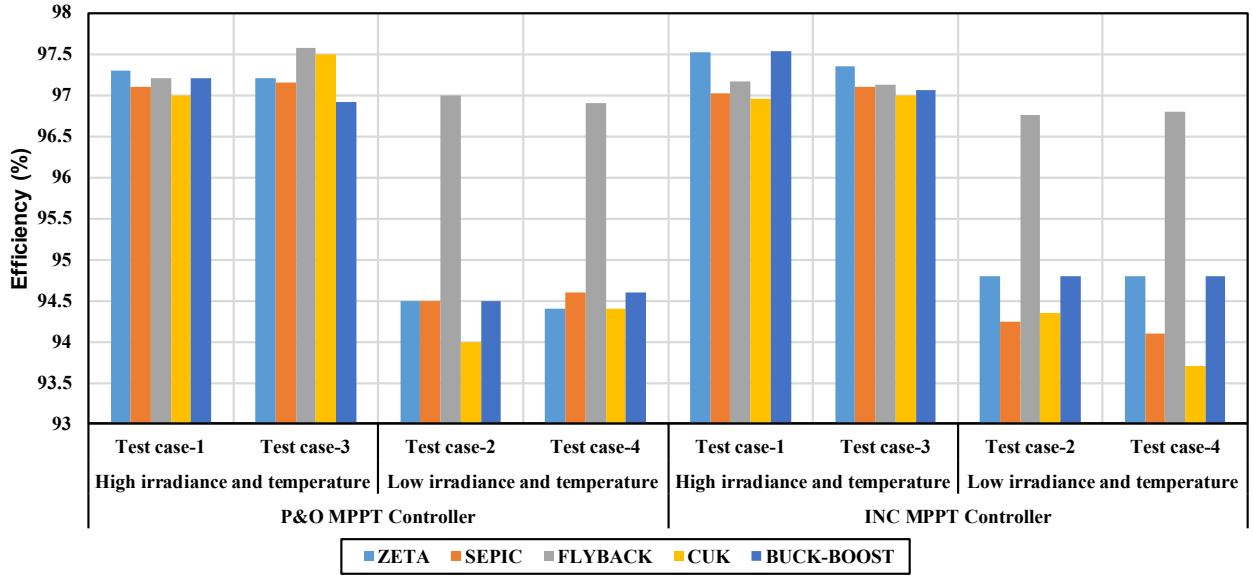

Fig. 35. Cumulative performance comparison of various converters with respect to efficiency.

Acknowledgements

This work was supported by the Project Grant No: VIT-AP/SpoRIC/RGEMS/2023-24/002, sponsored by "Research Grant in Engineering, Management and Science (RGEMS)" scheme of VIT-AP University, Amaravati 522241, Andhra Pradesh, INDIA.

Author Contributions

S.M. was responsible for the conceptualization, validation, resources, data curation, software development, and project administration. S.M. and Y.V.P.K. jointly contributed to the methodology, formal analysis, investigation, and original draft preparation. Y.V.P.K. was responsible for the review and editing, visualization, supervision, and funding acquisition. All authors have read and agreed to the published version of the manuscript.

Conflict of Interest

The author(s) declared no potential conflicts of interest with respect to the research, authorship, and/or publication of this article.

References

[1] C. Luo, Y.-F. Huang, and V. Gupta, "Stochastic dynamic pricing for EV charging stations with renewable integration and energy storage," IEEE Trans. Smart Grid, vol. 9, no. 2, pp. 1494–1505, Mar. 2018, doi:10.1109/TSG.2017.2696493.

[2] I. Akhtar, M. Jameel, A. Altamimi, and S. Kirmani, "An innovative reliability oriented approach for restructured power system considering the impact of integrating electric vehicles and renewable energy resources," IEEE Access, vol. 10, pp. 52358–52376, 2022, doi:10.1109/ACCESS.2022.3174365.

[3] B. R. Siddharth, V. S. Chandu, D. M. Babu, D. J. Pradeep, and Y. P. Kumar, "Performance analysis of hybrid electric vehicle architectures under dynamic operating conditions," Int. J. Adv. Sci. Technol., vol. 29, no. 10S, pp. 4370–4390, 2020.

[4] B. R. Siddharth, D. J. Pradeep, Y. P. Kumar, C. P. Reddy, and A. Flah, "Dynamic performance analysis of front-wheel drive hybrid electric vehicle architectures under different real-time operating conditions," Int. J. Powertrains, vol. 11, no. 1, pp. 62–89, 2022, doi:10.1504/IJPT.2022.121974.

[5] D. Potnuru, T. S. L. V. Ayyarao, L. V. S. Kumar, Y. V. P. Kumar, D. J. Pradeep, and C. P. Reddy, "Sap swarm algorithm based optimal speed control for electric vehicles," Int. J. Power Electron. Drive Syst., vol. 13, no. 2, pp. 755–763, 2022, doi:10.11591/ijpeds.v13.i2.pp755-763.

[6] D. J. Pradeep, Y. V. P. Kumar, B. R. Siddharth, C. P. Reddy, M. Amir, and H. M. Khalid, "Critical performance analysis of four-wheel drive hybrid electric vehicles subjected to dynamic operating conditions," World Electr. Veh. J., vol. 14, no. 6, p. 138, 2023, doi:10.3390/wevj14060138.

[7] B. Prasanth, R. Paul, D. Kaliyaperumal, R. Kannan, Y. V. P. Kumar, M. K. Chakravarthi, and N. Venkatesan, "Maximizing regenerative braking energy harnessing in electric vehicles using machine learning techniques," Electronics, vol. 12, no. 5, p. 119, 2023, doi:10.3390/electronics12051119.

[8] A. Pamidimukkala, S. Kermanshachi, J. Michael, and G. Hladik, "Evaluation of barriers to electric vehicle adoption: A study of technological, environmental, financial, and infrastructure factors," Transp. Res. Interdiscip. Perspect., vol. 22, p. 100962, Nov. 2023, doi:10.1016/j.trip.2023.100962.

[9] X. Zhao, H. Hu, H. Yuan, and X. Chu, "How does the adoption of electric vehicles reduce carbon emissions? Evidence from China," Heliyon, vol. 9, p. e20296, 2023, doi:10.1016/j.heliyon.2023.e20296.

[10] P. V. S. Aditya and S. J. Rubavathy, "VSI controller integrated DC–DC converter for electrical vehicle charging system in PV solar grid," Electr. Power Compon. Syst., pp. 1–14, 2023, doi:10.1080/15325008.2023.2270593.

[11] J. Šimko, M. Praženica, R. Koňarik, P. Koteš, "The analysis, modeling, and control of the forward DC/DC converter for the electric vehicle," Transp. Res. Procedia, vol. 74, pp. 831–837, 2023, doi:10.1016/j.trpro.2023.11.214.

[12] P. Boat and P. Boat, "A novel energy storage system for efficiency improvement of fuel cell electric vehicles based on a new high step-up DC–DC converter," AEUE – Int. J. Electron. Commun., vol. 175, p. 155077, 2024, doi:10.1016/j.aeue.2023.155077.

[13] S. Kim, H. Cha, H. Kim, and S. Kim, "High-efficiency voltage balancer having DC–DC converter function for EV charging station," IEEE J. Emerg. Sel. Top. Power Electron., vol. 9, no. 1, pp. 812–821, 2021, doi:10.1109/JESTPE.2019.2963124.

[14] Y. Yasa, "A system efficiency improvement of DC fast-chargers in electric vehicle applications: Bypassing second-stage full-bridge DC–DC converter in high-voltage charging levels," Ain Shams Eng. J., vol. 14, no. 9, p. 102391, 2023, doi:10.1016/j.asej.2023.102391.

[15] H. Saleeb, K. Said, A. Kassem, and R. Mostafa, "Control and analysis of bidirectional interleaved hybrid converter with coupled inductors for electric vehicle applications," Electr. Eng., vol. 102, no. 1, pp. 195–222, 2020, doi:10.1007/s00202-019-00860-3.

[16] R. Regis, D. M. Fernando, L. Tofoli, S. Daher, F. L. M. Antunes, and M. Antunes, "Interleaved bidirectional DC–DC converter for electric vehicle applications based on multiple energy storage devices," Electr. Eng., vol. 102, no. 4, pp. 2011–2023, 2020, doi:10.1007/s00202-020-01009-3.

[17] S.M. Shariff, M.S. Alam, F. Ahmad, Y. Rafat, M.S.J. Asghar, S. Khan, "System design and realization of a solar-powered electric vehicle charging station," IEEE Syst. J., vol. 14, no. 2, pp. 2748–2758, 2020, doi:10.1109/JSYST.2019.2931880.

[18] K. Yung and H. Hung, "Solar energy-powered battery electric vehicle charging stations: Current development and future prospect review," Renew. Sustain. Energy Rev., vol. 169, p. 112862, 2022, doi:10.1016/j.rser.2022.112862.

[19] A. Dick, S. Omer, and R. Boukhanouf, "Investigation of cost-effective electric vehicle charging station assisted by photovoltaic solar energy system," Transp. Res. Procedia, vol. 70, pp. 423–432, 2023, doi:10.1016/j.trpro.2023.11.048.

[20] M. Tan and T. Erdin, "Integration analysis of electric vehicle charging station equipped with solar power plant to distribution network and protection system design," J. Electr. Eng. Technol., vol. 17, no. 2, pp. 903–912, 2022, doi:10.1007/s42835-021-00927-x.

[21] S. Wang, Y. Li, and J. Jia, "How to promote sustainable adoption of residential distributed photovoltaic generation in China? An employment of incentive and punitive policies," Mitig. Adapt. Strateg. Glob. Change, vol. 27, no. 16, pp. 1–26, 2022, doi:10.1007/s11027-021-09977-y.

[22] A. Sangswang, M. Konghirun, and S. Member, "Optimal strategies in home energy management system integrating solar power, energy storage, and vehicle-to-grid for grid support and energy efficiency," IEEE Trans. Ind. Appl., vol. 56, no. 5, pp. 5716–5728, 2020, doi:10.1109/TIA.2020.2991652.

[23] A. Ameur, A. Berrada, and A. Emrani, "Intelligent energy management system for smart home with grid-connected hybrid photovoltaic/gravity energy storage system," J. Energy Storage, vol. 72, p. 108525, 2023, doi:10.1016/j.est.2023.108525.

[24] M. Kunjuramakurup, L. Sulthan, S. M. Ponparakkal, V. Raj, and S. Sathyajith, "A high-power solar PV-fed TISO DC–DC converter for electric vehicle charging applications," Energies, vol. 16, p. 2186, 2023.

[25] Pradeep Vishnuram, R. Narayanamoorthi, P. Suresh, K. Vijayakumar, M. Bajaj, T. Khurshaid, A. Nauman, S. Kamel, "A comprehensive review of EV power converter topologies, charger types, infrastructure and communication techniques," Front. Energy Res., vol. 11, pp. 1–17, 2023, doi:10.3389/fenrg.2023.1103093.

[26] G. M. Madhu and C. Vyjayanthi, "Investigation of effect of irradiance change in maximum power extraction from PV array interconnection schemes during partial shading conditions," IEEE Access, vol. 9, pp. 96995–97009, 2021, doi:10.1109/ACCESS.2021.3095354.

[27] N. Kumar, "Framework of maximum power extraction from solar PV panel using self predictive perturb and observe algorithm," IEEE Trans. Sustain. Energy, vol. 9, no. 2, pp. 895–903, 2018, doi:10.1109/TSTE.2017.2764266.

[28] V. Bhan, S. Ahmed, S. Zahid, H. Khan, T. Ahmed, and L. Ali, "Performance evaluation of perturb and observe algorithm for MPPT with buck-boost charge controller in photovoltaic systems," J. Control Autom. Electr. Syst., vol. 32, no. 6, pp. 1652–1662, 2021, doi:10.1007/s40313-021-00781-2.

[29] M. J. Dushmanta and K. Das, "A novel adaptive model predictive control scheme with incremental conductance for extracting maximum power from a solar panel," Iran. J. Sci. Technol. Trans. Electr. Eng., vol. 46, no. 3, pp. 653–664, 2022, doi:10.1007/s40998-022-00495-4.

[30] S. F. Chevtchenko, E. J. Barbosa, M. C. Cavalcanti, G. M. S. Azevedo, and T. B. Ludermir, "Combining PPO and incremental conductance for MPPT under dynamic

shading and temperature," Appl. Soft Comput., vol. 131, p. 109748, 2022, doi:10.1016/j.asoc.2022.109748.

[31] S. Kumar, G. Shanmugam, T. S. Sakthivel, B. A. Gaftar, P. Iyyappan, and R. Sathyamurthy, "Modeling and simulation of single- and double-diode PV solar cell model for renewable energy power solution," Environ. Sci. Pollut. Res., vol. 29, pp. 4414–4430, 2022, doi:10.1007/s11356-021-15870-7.

[32] S. Mamidala, A. K. Prajapati, and S. Ravada, "Modeling of buck converter charging station to improve the power quality using three phase single tuned harmonic filter for electric transportation," in Proc. 2022 IEEE 2nd Int. Conf. Sustainable Energy and Future Electric Transportation (SeFeT), 2022, pp. 1–6, doi:10.1109/SeFeT55524.2022.9909306.

[33] R. Pandey, "A Cuk converter and resonant LLC converter based e-bike charger for wide output voltage variations," IEEE Trans. Ind. Appl., vol. 57, no. 3, pp. 2682–2691, 2021, doi:10.1109/TIA.2021.3066089.

[34] P. K. Maroti, S. Padmanaban, M. Meraj, A. Iqbal, and S. Mekhilef, "A new structure of high voltage gain SEPIC converter for renewable energy applications," IEEE Access, vol. 7, pp. 89857–89868, 2019, doi:10.1109/ACCESS.2019.2925564.

[35] M. Veerachary and M. R. Khuntia, "Design and analysis of two-switch-based enhanced gain buck-boost converters," IEEE Trans. Ind. Electron., vol. 69, no. 4, pp. 3577–3587, 2022, doi:10.1109/TIE.2021.3071696.

[36] R. Kushwaha and B. Singh, "Bridgeless isolated zeta–luo converter-based EV," IEEE Trans. Ind. Appl., vol. 57, no. 1, pp. 628–636, 2021, doi:10.1109/TIA.2020.3036019.

[37] N. T. Milas and E. C. Tatakis, "Fast battery cell voltage equalizer based on the bidirectional flyback converter," IEEE Trans. Transp. Electrific., vol. 9, no. 4, pp. 4922–4940, 2023, doi:10.1109/TTE.2022.3186520.

[38] H. Bousmaha, M. Flitti, and P. R. Sanchez, "MPPT algorithm with a closed-loop control of the input voltage of a boost converter in PV systems," in Proc. 11th Int. Conf. Renewable Energy Research and Applications (ICRERA), Istanbul, Turkey, 2022, pp. 107–111, doi:10.1109/ICRERA55966.2022.9922766.

[39] B. Sarsembayev, N. Zhakiyev, A. Akhmetbayev, and K. Kayisli, "Servomechanism based optimal control system design for maximum power extraction from WECS with PMSG," in Proc. 10th Int. Conf. Smart Grid (icSmartGrid), Istanbul, Turkey, 2022, pp. 309–313, doi:10.1109/icSmartGrid55722.2022.9848769.

[40] M. Chellal, T. F. Guimaraes, and V. Leit, "Experimental evaluation of MPPT algorithms: A comparative study," Int. J. Renewable Energy Res., vol. 11, no. 1, 2021, doi:10.20508/ijrer.v11i1.11797.g8164.

[41] R. Z. Caglayan, K. Kayisli, N. Zhakiyev, A. Harrouz, and I. Colak, "A review of hybrid renewable energy systems and MPPT methods," Int. J. Smart Grid, vol. 6, no. 3, Sep. 2022, doi:10.20508/ijsmartgrid.v6i3.248.g243.

[42] J. Dey, N. Mohammad, and M. T. Islam, "Analysis of a microgrid having solar system with maximum power point tracking and battery energy system," in Proc. 10th Int. Conf. Smart Grid (icSmartGrid), Istanbul, Turkey, 2022, pp. 179–184, doi:10.1109/icSmartGrid55722.2022.9848553.

[43] H. Shams, J. Yu, and A. W. Shamas, "Modeling and simulation of PV system with three phase inverter along PV, IV curves using MATLAB/Simulink," Int. J. Smart Grid, vol. 7, no. 4, Dec. 2023, doi:10.20508/ijsmartgrid.v7i4.309.g303.